2. Materials and methods

2.1. Synthetic peptides

The Tax11-19 peptide, LLFGYPVYV, was purchased from Asahi Technoglass (Chiba, Japan) and used as an HLA-A2-restricted CTL antigen [11].

2.2. Cells

C1R.AAD cell line (HMYC1R transfected with HLA chimeric molecule containing α1 and α2 domains from human HLA-A2.1 and α3 from mouse H-2D^d) was described previously [22]. Cell lines were maintained in culture medium (CTM; 1:1 mixture of RPMI 1640 and Eagle-Hank's amino acid (EHAA)) containing 10% fetal bovine serum (FBS), 1 mM sodium pyruvate, 0.1 mM nonessential amino acids, 10 mM HEPES, 4 mM glutamine, 100 U/ml penicillin, and 100 μg/ml streptomycin.

HTLV-1-infected human ATL cell lines, KK-1 and KOB, were derived from the peripheral blood and ascites of ATL patients, respectively [23,24]. Human IL-2 dependent T cell line (HCT-4) was derived from the cerebrospinal fluid of a HAM/TSP patient [25]. KK-1, KOB, and HCT-4 were used as a target. Cells were maintained in CTM with 100 units/ml of recombinant human IL-2 (Imunace®35, Shionogi, Osaka, Japan).

2.3. Mice

Transgenic HHD-2 mice (gift from Dr. François Lemonnier, Institute Pasteur, Paris, France) were bred in our colony at the Institute of the Experimental Animals at St. Marianna University. HHD-2 mice are characterized by knock-out of the murine β_2-microglobulin gene, as well as murine H-2D^b, transgenic expression of human HLA-A2.1 with a covalently-linked human β_2-microglobulin and a murine D^b-derived α3 domain to allow interaction with mouse CD8 [26]. All animal studies were approved by the Institute of Experimental animals at St. Marianna University.

2.4. Binding assay

Peptide binding to HLA-A2 molecules was measured using T2 mutant cell lines as described previously [27,28]. T2 cells (3×10^5/well) were incubated overnight in 96-well plates with culture medium (a 1:1 mixture of RPMI 1640 and Eagle-Hank's amino acid (EHAA) containing 2% FBS, 100 U/ml penicillin, 100 mg/ml streptomycin) with 10 μg/ml human β_2-microglobulin (Sigma–Aldrich, St. Louis, MO) and different peptide concentration. On the following day, cells were washed at 190 × g for 5 min twice with cold PBS containing 2% FBS and incubated for 30 min at 4 °C with anti-HLA-A2.1 BB7.2 mAb (1/100 dilution of hybridoma supernatant) and 5 μg/ml FITC-labeled goat anti-mouse Ig (BD PharMingen, San Diego, CA). Cells were washed twice after each incubation; subsequently, HLA-A2.1 expression was measured by flow cytometry (FACScan; BD Biosciences, Mountain View, CA). HLA-A2.1 expression was quantified as fluorescence index (FI) according to the formula: FI = ((geometric mean fluorescence with peptide − geometric mean fluorescence without peptide)/geometric mean fluorescence without peptide). $FI_{0.5}$ is the concentration required to give an FI of 0.5, meaning a 50% increase in HLA-A2 on the cell surface. Background fluorescence without BB7.2 was subtracted for each individual value. To compare the different peptides, $FI_{0.5}$ was calculated from the titration curve for each peptide. Each sample was tested in triplicate. Values were expressed as mean in triplicate.

2.5. CTL generation in HHD-2 transgenic mice

The method for generating antigenic peptide-specific CTL lines form HHD mice was described previously [28,29]. Mice aged more than 8 weeks were immunized subcutaneously in the base of the tail with 100 μl of an emulsion containing 1:1 incomplete Freund's adjuvant (IFA), antigenic CTL peptide and cytokines (50 nmol Tax (11-19) peptide, 25 nmol HBV core 128–140 helper epitope, 3 μg of rmIL-12 and 3 μg of rmGM-CSF). Mice were boosted 2 weeks later, with the spleens removed 10–14 days after the boost. Immune spleen cells (2.5×10^6/well) were stimulated in 24-well plates with autologous spleen cells (5×10^6/well) pulsed for 30 min with 10 μM Tax11-19 peptide for the development of low-avidity CTL lines (LCTL) or with 10 nM for high-avidity CTL lines (HCTL) in CTM supplemented with 10% T-stim® (Collaborative Biochemical Products, Bedford, MA). Following a minimum of four in vitro stimulations with the peptide-pulsed syngeneic spleen cells, two CTL lines were maintained by weekly restimulation with 1×10^6 cells/well with 4×10^6 peptide-pulsed mitomycin C-treated syngeneic spleen cells as feeders.

2.6. Cytotoxic assay

CTL activity was measured with ^{51}Cr-labeled target cells. Target cells (1×10^6) were pulsed in 100 μl of 150 μCi ^{51}Cr for 1 h and were washed three times, with 5000 cells/well then added to 96-well round-bottom plates containing different peptide concentrations. Effector cells were introduced followed by additional incubation. Supernatants were then harvested and analyzed. The percentage of specific ^{51}Cr release was calculated as 100 × (experimental release − spontaneous release)/(maximum release − spontaneous release). Spontaneous release was determined from target cells that had been incubated in the absence of effector cells, while maximum release was determined in the presence of 2% TRITON® X-100 Detergent (CALBIOCHEM, La Jolla, CA). Each sample was tested in triplicate. Values were expressed as means ± SEM of triplicates.

2.7. IFN-γ ELISA assay

IFN-γ in the culture supernatant harvested at 24 h was determined using an ELISA kit (R&D, Minneapolis, MN) according to the manufacture's instructions. All samples were analyzed in triplicate. Values were expressed as means ± SEM of triplicates.

2.8. TCR Vβ screenings of CTLs

We assessed a Vβ usage pattern between HCTL and LCTL using Vβ TCR screening kit by a flow cytometry analysis (BD Bioscience Phamingen, San Diego, CA).

2.9. Flow cytometry

We used a PE-Tax11-19/HLA-A*0201 tetramer-LLFGYPVYV (Medical & Biological Laboratories, Nagoya, Japan) and PE-hamster anti-mouse CD3ε Ab (145-2C11, BD Bioscience Phamingen, San Diego, CA). Cells were centrifuged and washed twice with PBS containing 0.5% BSA, and then resuspended in 1% BSA/PBS. Cells were incubated 40 min at 4 °C with the antibody and then washed three times. The tetramer and anti CD3ε Ab were titrated for staining simultaneously.

In order to compare the affinity of T cell receptor between HCTLs and LCTLs, indexes were calculated using the following two equations: ratio of geometric mean (RGM) = (geometric mean using tetramer or anti-CD3ε Ab)/(geometric mean using control Ab). Each sample was tested in triplicate.

2.10. Western blotting

KK-1, KOB, and HCT-4 were lysed using standard lysis buffer (20 mM Tris–HCl, 250 mM NaCl, 1% NP-40, 1 mM dithiothreitol, 10 mM NaF, 2 mM Na_3VO_4, 10 mM $Na_4P_2O_7$, and protease inhibitor cocktail (Roche, Mannheim, Germany)). Lysates were stored at −80 °C until use. Protein concentration was determined using the Bradford method (Bio-Rad protein assay reagent; Bio-Rad laboratories, Hercules, CA). Equal amounts (30 μg) of protein were separated by SDS–PAGE on 10% polyacrylamide gels and transferred to PVDF membranes. Following the transfer, membranes were blocked with Difco Skim milk (BD Bioscience, San Diego, CA) overnight at 4 °C. The working concentrations of the first Abs were 1 μg/ml for anti-Tax Ab (Lt-4) [30] and anti murine β-actin Ab (SIGMA, St. Louis, MO), and 1:10,000 for HRP-conjugated anti-mouse IgG Ab (SIGMA, St. Louis, MO). The membrane was washed, and was reacted with the appropriate second antibody. Finally, signals were visualized using the extended cavity laser (ECL) system (GE Healthcare Bio-sciences KK, Tokyo, Japan).

2.11. Real-time reverse transcriptase-PCR (RT-PCR)

Total RNA was isolated from cells using TRIzol® Reagent (Invitrogen, Carisbad, CA). First-stand cDNA was synthesized with random hexamers and reverse transcriptase (ReverTraAce; Toyobo, Japan) using 1 μg of total RNA in a reaction volume of 20 μl. Real-time PCR reactions were carried out using TaqMan® Universal Master Mix (Applied Biosystems, Carisbad, CA). ABI Prism 7500 SDS was programmed to an initial step of 2 min at 50 °C and 10 min at 95 °C, followed by 45 cycles of 15 s at 95 °C and 1 min at 60 °C. The primers and probe for detecting the HTLV-1 Tax or GAPDH mRNA were used as described previously [31]. Relative quantification of mRNA was performed using the comparative threshold cycle method with GAPDH as an endogenous control. For each sample, target gene expression was normalized against the expression of GAPDH. To determine relative expression levels, the following formula was used: target gene expression = $2^{-(Ct[target]-Ct[GAPDH])}$. Each sample was tested in triplicate. Values were expressed as means ± SEM of triplicates.

3. Results

3.1. Binding affinity of Tax11-19 for HLA-A2 molecule

Before attempting to develop Tax-specific CTL lines from HLA-A2 transgenic HHD mice, we evaluated the binding affinity of Tax11-19 peptide by T2 binding assay, which measures the cell surface stabilization of HLA-A2 molecules. Tax11-19 peptide displayed a binding capacity for the HLA-A2 molecule that was nearly equal to that of the positive control, the highly antigenic influenza virus matrix peptide (FMP58-66) [32] ($FI_{0.5}$ = 0.329 for Tax11-19, 0.284 μM for FMP58-66) (Fig. 1). These data suggest that Tax11-19 would be a very strong antigenic peptide restricted to the HLA-A2 molecule.

3.2. Recognition of Tax11-19 peptide by CTL lines of different avidity

Based on the observation that Tax11-19 showed strong antigenicity inducing specific CTLs, we next attempted to develop low-avidity CTLs (LCTL) and high-avidity CTLs (HCTL) from HLA-A2 transgenic mice. HCTL were generated by weekly stimulation using low concentrations (10 nM) of the Tax peptide pulsed onto APCs, while LCTLs were also generated using 10 μM of the Tax peptide pulsed onto APCs. Using these different CTL lines, we examined Tax-specific CTLs-mediated cytotoxicity with Tax peptide titrated over a range of concentrations. The titration curve showed a

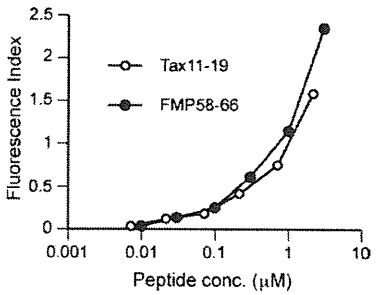

Fig. 1. Comparison of HLA-A2 binding curves between Tax11-19 and FMP58-66 peptide in T2-binding assay. The binding affinity of Tax11-19 for HLA-A2 molecule is almost as strong as that of FMP58-66 in influenza A virus.

0.5–1 $\log_{10}$ difference in functional avidity measured as the peptide concentration necessary to produce 50% lysis (Fig. 2A). Similarly, we examined their properties in antigen-specific IFN-γ production from these CTL lines (Fig. 2B). With a 24 h assay, HCTLs showed more IFN-γ production than LCTLs even at lower concentration of Tax antigen. These data suggest that the two different CTL lines specific for Tax have different functional avidity.

3.3. Different Vβ usage and binding ability to Tax-tetramer between high- and low-avidity CTLs

In order to confirm whether these CTLs with different avidity possessed different TCR structures, we assessed the difference in Vβ usage pattern between HCTLs and LCTLs using flow cytometric analysis (FCM). On FCM, antibodies available for screening were those for Vβ 2, 3, 4, 5, 6, 7, 8.1, 8.2, 8.3, 9, 10, 11, 12, 13, 14, and 17. On FCM, no Vβ were detected in LCTLs, while only Vβ5 was detected in HCTLs (Fig. 3A). The data suggested that the major TCR repertoire of HCTL is Vβ5, indicating that these two Tax-specific CTL lines have different TCR structures.

We next compared the binding affinity of TCR between HCTL and LCTL using Tax11-19/HLA-A2 tetramer-LLFGYPVYV and anti-CD3 Ab (Fig. 3B). On FCM with both Tax11-19-tetramer and anti-CD3 Ab titration, HCTLs showed a stronger fluorescence than LCTLs (Fig. 3B). On Tax11-19-tetramer assay, the ratio of fluorescence index (HCTL/LCTL) was ~5-fold at any titrated concentration, and it took 1.5 logs more tetramer to achieve the same level of staining. In the titration of anti-CD3 Ab, the ratio was ~3-fold and also it required about 3-fold more antibody to reach the same level of staining. These findings suggested that HCTLs not only have higher TCR affinity but also express greater numbers of TCR molecules on their surface when compared with LCTLs.

3.4. Recognition of human ATL targets by Tax-specific CTLs from HHD mice

We further examined whether these murine CTL lines with different functional avidity could induce cytotoxic activity against human ATL targets. We used the HTLV-1-infected human ATL cell lines, KK-1 (HLA-A2) and KOB (HLA-A30) as target cells derived from peripheral blood and ascitis of ATL patients, respectively [23,24]. These murine CTL lines did not show strong cytotoxicity against human ATL lines as against murine targets with a 4 h assay, as it was previously reported that species specificity between murine CD8 and the α3 domain of human HLA-A2 may reduce the recognition ability by CTLs [33]. However, on a 12 h assay, cytotoxicity against human ATL was observed in an HLA-A2 restricted manner (Fig. 4A). HCTLs were especially more efficient at killing at low E/T ratios. Furthermore, on kinetics assay, HCTLs showed more efficient cytotoxicity against the human ATL target (KK-1) than LCTLs (Fig. 4B).

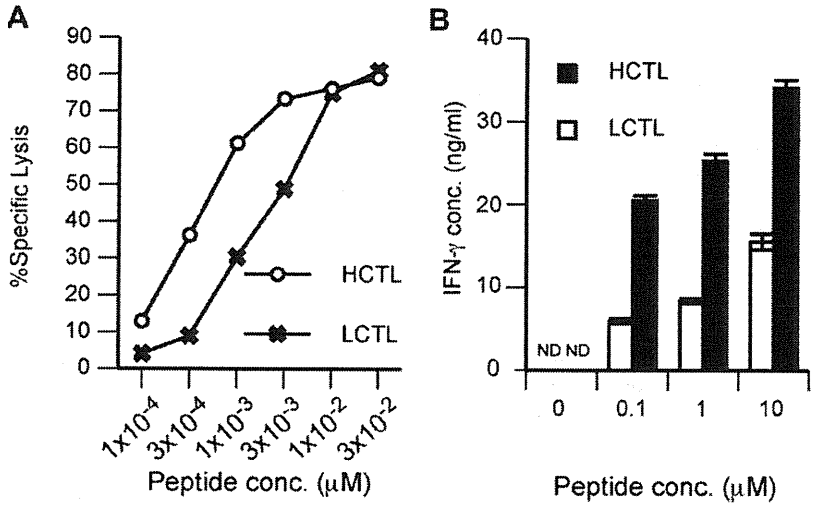

Fig. 2. Difference in functional avidity between HCTLs and LCTLs. (A) Recognition by the Tax11-19 peptide specific CTLs, HCTL and LCTL, of Tax11-19 antigenic peptide from 10^{-4} to 10 μM when presented on C1R.AAD target cells. The effector to target-cell (E/T) ratio was 20:1. Error bars were omitted because all SEMs were <3.5%. (B) Comparison of Tax11-19-specific IFN-γ production between HCTLs and LCTLs. A total of 200,000 CTL cells were cultured with 100,000 mytomicin-c treated C1R.AAD cell with 0.1–10 μM Tax11-19 peptide. Culture supernatants at 24 h were assayed using IFN-γ ELISA kit according to the manufacturer's instructions. ND, not detected.

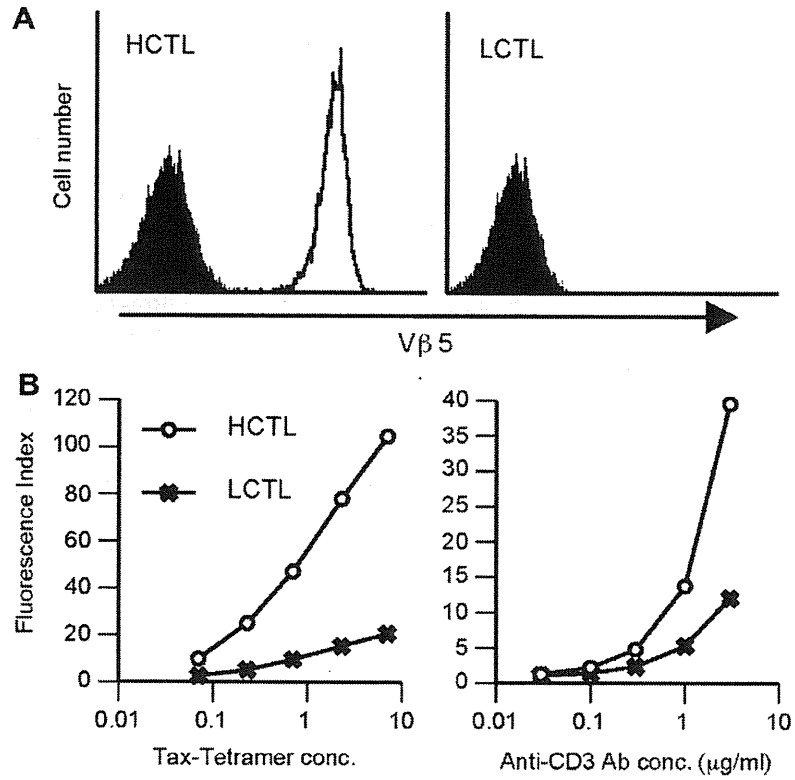

Fig. 3. TCR Vβ usage and expression level of TCR complex on Tax-specific CTLs with different functional avidity. (A) Comparison of Vβ usage pattern between HCTLs and LCTLs cytometry analysis (FCM). No Vβs among available anti-Vβ antibodies were detected in LCTL but only Vβ5 was detected in HCTL. (B) Comparison of binding curves for human Tax11-19-tetramer and anti-CD3ε Ab between HCTLs and LCTLs. HCTLs consistently showed a stronger fluorescence index than LCTLs; for Tax11-19-tetramer, the ratio of fluorescence index (LCTL/HCTL) was ~5-fold, and for anti-CD3ε Ab, it was ~3-fold.

3.5. Recognition of HTLV-1 infected human T cells by Tax-specific CTL from HHD mice

Next, in order to examine a comparison of the cytotoxicity against HTLV-1 infected non-tumor cells, we used HTLV-1 infected human T cells (HCT-4) derived from a patient with HAM/TSP [25]. On a 12 h lytic assay, HCTLs showed more efficient cytotoxicity against the HTLV-1 infected human T cells while LCTLs were not able to kill the targets under the these experimental conditions (Fig. 5A). At no time point was there detectable killing by LCTLs (Fig. 5B). These findings suggested that the superior recognition ability by the CTLs with higher functional avidity may have a more

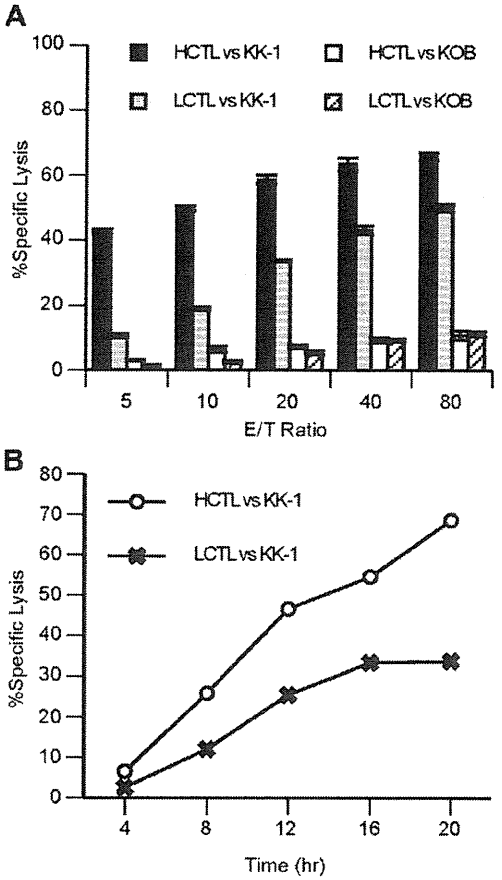

Fig. 4. Recognition pattern of human ATL targets by Tax-specific CTLs. (A) Comparison of cytotoxicity for human ATL targets (KK1, HLA-A2; KOB, HLA-A30) between HCTLs and LCTLs. (12 h ^{51}Cr release assay) (B) Comparison of kinetics of Tax-specific CTL-mediated cytotoxicity (E:T ratio = 40:1) between HCTLs and LCTLs. Similar results were obtained in three different experiments.

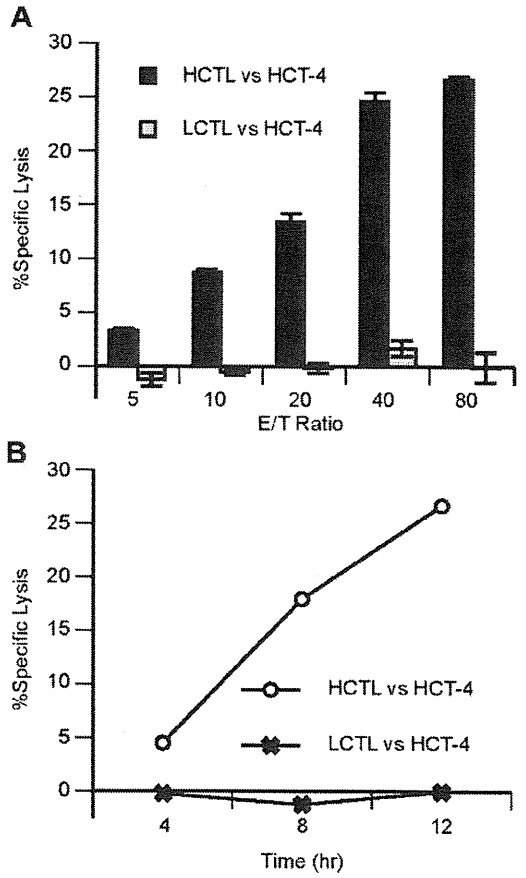

Fig. 5. Recognition pattern of HTLV-1 infected human T cell line by Tax-specific CTLs. (A) Comparison of cytotoxicity for human IL-2 dependent HTLV-1 infected cell, HCT-4 (HLA-A2), between HCTLs and LCTLs. (12 h ^{51}Cr release assay). (B) Comparison of kinetics of Tax-specific CTL-mediated cytotoxicity (E:T = 40:1) between HCTLs and LCTLs. Similar results were obtained in four different experiments.

striking effect in the case of recognizing normal cells infected with the virus.

3.6. Expression of Tax product in human ATL tumors and HTLV-1 infected T cell target

The cytotoxicity data against human targets indicated that higher functional avidity in CTLs is critical for efficient cytotoxicity against tumor or infected normal cell targets in humans. However, the amount of Tax antigen expressed in target cells that could be recognized by higher avidity CTLs was unclear. Therefore, we investigated how much Tax products could be yielded in these human ATL and HTLV-1 infected target cells. Using western blotting (Fig. 6A), Tax protein was detected in KOB and HCT-4 target cells, but not in KK-1. Since KK-1 cells were recognized by HCTLs more strongly than by LCTLs, we further evaluated the level of Tax mRNA produced in KK-1 using real-time PCR. The expression levels of Tax mRNA in KK-1 were around one thousand-fold lower than that in KOB (Fig. 6B). These results demonstrated that Tax11-19-specific higher avidity CTLs showed more efficient cytotoxicity against ATL by recognizing very small amount of Tax product detected only with real-time PCR.

4. Discussion

HTLV-1 infection elicits a strong CTL response, with Tax protein being the major target of HTLV-1-specific CTLs [10,11]. In the field of anti-tumor immunity, the in vivo relevance of differences in functional avidity has been established by demonstrating that high-avidity CTLs clear tumor antigens more efficiently than low-avidity CTL [34–38]. In HTLV-1 infection, however, while there is increasing body of evidence that CTL quality from the aspect of functional avidity of CTL might be crucial for the efficient control of HTLV-1 infection [17,39], little is known about how the functional avidity of HTLV-1 virus-specific CTLs is related to the control of HTLV-1-infected cells and tumors. Furthermore, the virus is latent in the tumor cells and it is difficult to detect expression of viral proteins [40–42]. This is the reason why there has not been direct evidence on whether Tax11-19 works as a definitive CTL antigen in HLA-A2-restricted patients with HTLV-1 infection and ATLs. The present study provides clear evidence regarding the notion that high avidity CTLs specific for Tax protein play a greater role in the specific destruction of ATL and HTLV-1-infected cells using Tax-specific CTLs with different functional avidity generated from HLA-A2 transgenic HHD mice, with human ATL lines and HTLV-1 infected cells acting as targets. As Tax11-19 peptide antigen binds HLA-A2 with almost as high affinity as FMP58-66 in influenza A virus (Fig. 1), which has one of the highest affinity peptides among HLA-A2 restricted peptide antigens [27,28], we developed CTL lines specific for Tax11-19, HCTL and LCTL, for which we found the optimum antigen-presenting conditions for the induction and maintenance of the CTL lines were 10 nM- and

10 μM-peptide pulsing APCs, respectively. The 1000-fold difference of such antigenic concentration resulted in the CTL lines with differences of functional avidity in antigen-specific cytotoxicity and IFN-γ production (Fig. 2). These different avidity CTLs also had different repertoires of TCRVβ, suggesting the structure of TCR in the major repertoire of two lines were distinct (Fig. 3A). In order to compare TCR affinity for the human Tax-tetramer, the mismatch of which to murine CD8 could permit assessment of the strength of TCR ligation to peptide/MHC complex more closely without the influence of CD8 binding [43], we titrated the tetramer and evaluated the effect of the number of TCR molecules expressed at the same time. Higher avidity Tax-specific CTLs showed higher fluorescene on both Tax-tetramer (~5-fold) and anti-CD3Ab (~3-fold) staining (Fig. 3B), thus suggesting that CTL might acquire higher avidity state by possessing the different structure of the TCR as well as by increasing the number of TCR molecules expressed although other factors could also play a role for determining the avidity of CTLs [15].

HTLV-1 Tax, a critical viral protein for HTLV-1 leukemogenesis, is the most likely target for HTLV-1 specific CTL in HTLV-1-infected individuals [10,11]. In HTLV-1-infected patients with HLA-A2, the Tax11-19-specific CTL response is predominantly detected in culture [44]. However, few details are known about the recognition mechanism by Tax-specific CTLs because of the difficulty of developing CTL lines specific for Tax11-19 antigen [9]. Although both HCTLs and LCTLs developed from HLA-A2 transgenic mice were not able to induce cytotoxicity against the human HLA-A2-restricted ATL line, KK-1, on 4 h assay because of the mismatch between the murine CD8 and human α3 domain [22], HCTLs clearly showed more efficient cytotoxicity than LCTLs with longer-term assay of more than 4 h (Fig. 4). Furthermore, the use of the human IL-2-dependent HTLV-1-infected non-tumor cell, HCT-4, clearly brought out the difference in cytotoxic efficacy between HCTL and LCTL (Fig. 5). These findings could be direct evidence not only that Tax11-19 might be naturally processed for presentation as a CTL antigen in both ATL tumor cells and virus-infected cells but also that the higher avidity CTL for Tax11-19 could be more critical in clearing HTLV-1-infected cells as well as ATL tumors in HLA-A2-restricted patients. In addition, HCTLs could more strongly recognize a latent level of Tax product detected only with a real-time PCR, not detectable with western blotting in the ATL target (Fig. 6). Furthermore, HCTLs also possessed higher elimination potential against HTLV-1 infected non-tumor targets when compared with LCTLs (Figs. 4 and 5).

The present findings are consistent with previous reports showing that the lytic efficiency of $CD8^+$ T cell response was inversely correlated with the proviral load and the rate of proviral expression in patients with HTLV-1 infection [17]. These data also strongly support the notion that induction of high avidity CTLs is critical for development of more effective vaccines against cancer and chronic viral infection such as HTLV-1and HIV. In addition, based on the observation that the high-avidity CTLs expressed a greater number of TCR molecules when compared with the low-avidity CTLs (Fig. 3B), such more multivalent TCR display might be one of the critical factors in establishing functional high avidity, leading to more efficient TCR cell therapy in the future [45].

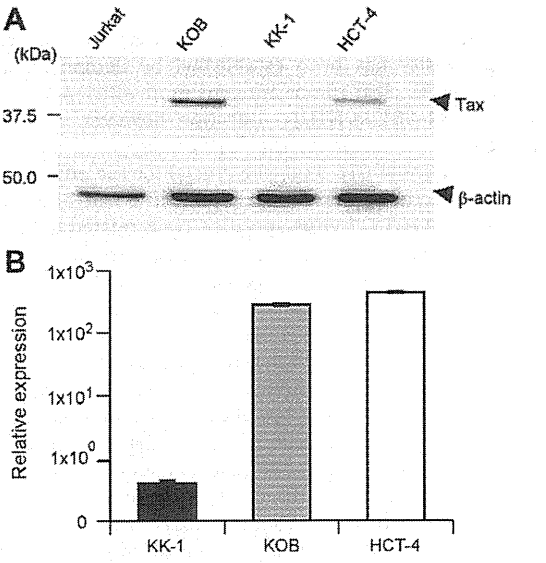

Fig. 6. Expression of Tax product in human ATL tumors and HTLV-1 infected T cell targets. (A) Tax protein is detected in KOB and HCT-4 by western blotting, but not in KK-1. Jurkat cells were used as a negative control. (B) Comparison of mRNA production of Tax by real-time PCR among KOB, KK-1 and HCT-4. Tax production in KK-1 was detected by real-time PCR, but not in a western blotting. Jurkat cells as a negative control gave no detectable signal with the Tax-primer.

Conflict of interest

The authors declare no conflict of interest.

Acknowledgments

We would like to thank Dr. Jay A. Berzofsky for critical reading of the manuscript and helpful suggestions. We also would like to thank Hiroe Ogasawara and Katsunori Takahashi for technical assistance provided during the study.

References

[1] Y. Hinuma, K. Nagata, M. Hanaoka, M. Nakai, T. Matsumoto, K.I. Kinoshita, S. Shirakawa, I. Miyoshi, Adult T-cell leukemia: antigen in an ATL cell line and detection of antibodies to the antigen in human sera, Proc. Natl. Acad. Sci. USA 78 (1981) 6476–6480.
[2] M. Yoshida, M. Seiki, K. Yamaguchi, K. Takatsuki, Monoclonal integration of human T-cell leukemia provirus in all primary tumors of adult T-cell leukemia suggests causative role of human T-cell leukemia virus in the disease, Proc. Natl. Acad. Sci. USA 81 (1984) 2534–2537.
[3] A. Gessain, F. Barin, J.C. Vernant, O. Gout, L. Maurs, A. Calender, G. De The, Antibodies to human T-lymphotropic virus type-I in patients with tropical spastic paraparesis, Lancet 2 (1985) 407–410.
[4] M. Osame, K. Usuku, S. Izumo, N. Ijichi, H. Amitani, A. Igata, M. Matsumoto, M. Tara, HTLV-I associated myelopathy, a new clinical entity, Lancet 1 (1986) 1031–1032.
[5] T. Matsuzaki, M. Nakagawa, M. Nagai, K. Usuku, I. Higuchi, K. Arimura, H. Kubota, S. Izumo, S. Akiba, M. Osame, HTLV-I proviral load correlates with progression of motor disability in HAM/TSP: analysis of 239 HAM/TSP patients including 64 patients followed up for 10 years, J. Neurovirol. 7 (2001) 228–234.
[6] M.A. Nowak, C.R. Bangham, Population dynamics of immune responses to persistent viruses, Science 272 (1996) 74–79.
[7] A.M. Vine, A.G. Heaps, L. Kaftantzi, A. Mosley, B. Asquith, A. Witkover, G. Thompson, M. Saito, P.K. Goon, L. Carr, F. Martinez-Murillo, G.P. Taylor, C.R. Bangham, The role of CTLs in persistent viral infection: cytolytic gene expression in CD8+ lymphocytes distinguishes between individuals with a high or low proviral load of human T cell lymphotropic virus type 1, J. Immunol. 173 (2004) 5121–5129.
[8] M. Kannagi, K. Sugamura, K. Kinoshita, H. Uchino, Y. Hinuma, Specific cytolysis of fresh tumor cells by an autologous killer T cell line derived from an adult T cell leukemia/lymphoma patient, J. Immunol. 133 (1984) 1037–1041.
[9] B. Arnulf, M. Thorel, Y. Poirot, R. Tamousa, E. Boulanger, A. Jaccard, E. Oksenhendler, O. Hermine, C. Pique, Loss of the ex vivo but not the reinducible CD8+ T-cell response to Tax in human T-cell leukemia virus type 1-infected patients with adult T-cell leukemia/lymphoma, Leukemia 18 (2004) 126–132.
[10] S. Jacobson, H. Shida, D.E. McFarlin, A.S. Fauci, S. Koenig, Circulating CD8+ cytotoxic T lymphocytes specific for HTLV-I pX in patients with HTLV-I associated neurological disease, Nature 348 (1990) 245–248.
[11] M. Kannagi, S. Harada, I. Maruyama, H. Inoko, H. Igarashi, G. Kuwashima, S. Sato, M. Morita, M. Kidokoro, M. Shigemoto, Predominant recognition of human T cell leukemia virus type I (HTLV-I) pX gene products by human CD8+ cytotoxic T cells directed against HTLV-I-infected cells, Int. Immunol. 3 (1991) 761–767.

[12] K.T. Jeang, Functional activities of the human T-cell leukemia virus type I Tax oncoprotein: cellular signaling through NF-kappa B, Cytokine Growth Factor Rev. 12 (2001) 207–217.
[13] M. Yoshida, Multiple viral strategies of HTLV-1 for dysregulation of cell growth control, Annu. Rev. Immunol. 19 (2001) 475–496.
[14] M. Kannagi, S. Matsushita, S. Harada, Expression of the target antigen for cytotoxic T lymphocytes on adult T-cell-leukemia cells, Int. J. Cancer 54 (1993) 582–588.
[15] M.A. Alexander-Miller, High-avidity CD8+ T cells: optimal soldiers in the war against viruses and tumors, Immunol. Res. 31 (2005) 13–24.
[16] M. Derby, M. Alexander-Miller, R. Tse, J.A. Berzofsky, High-avidity CTL exploit two complementary mechanisms to provide better protection against viral infection than low-avidity CTL, J. Immunol. 166 (2001) 1690–1697.
[17] T. Kattan, A. MacNamara, A.G. Rowan, et al., The avidity and lytic efficiency of the CTL response to HTLV-1, J. Immunol. 182 (9) (2009) 5723–5729.
[18] A. Gallimore, T. Dumrese, H. Hengartner, R.M. Zinkernagel, H.G. Rammensee, Protective immunity does not correlate with the hierarchy of virus-specific cytotoxic T cell responses to naturally processed peptides, J. Exp. Med. 187 (1998) 1647–1657.
[19] A.G. Cawthon, H. Lu, M.A. Alexander-Miller, Peptide requirement for CTL activation reflects the sensitivity to CD3 engagement: correlation with CD8ab versus CD8aa expression, J. Immunol. 167 (2001) 2577–2584.
[20] S. Walter, L. Herrgen, O. Schoor, G. Jung, D. Wernet, H.J. Buhring, H.G. Rammensee, S. Stevanovic, Cutting edge: predetermined avidity of human CD8 T cells expanded on calibrated MHC/anti-CD28-coated microspheres, J. Immunol. 171 (2003) 4974–4978.
[21] P.M. Gray, G.D. Parks, M.A. Alexander-Miller, High avidity CD8+ T cells are the initial population elicited following viral infection of the respiratory tract, J. Immunol. 170 (2003) 174–181.
[22] M.H. Newberg, D.H. Smith, S.B. Haertel, D.R. Vining, E. Lacy, V.H. Engelhard, Importance of MHC class 1 a2 and a3 domains in the recognition of self and non-self MHC molecules, J. Immunol. 156 (1996) 2473–2480.
[23] Y. Yamada, Y. Nagata, S. Kamihira, M. Tagawa, M. Ichimaru, M. Tomonaga, H. Shiku, IL-2-dependent ATL cell lines with phenotypes differing from the original leukemia cells, Leuk. Res. 15 (1991) 619–625.
[24] T. Maeda, Y. Yamada, R. Moriuchi, K. Sugahara, K. Tsuruda, T. Joh, S. Atogami, K. Tsukasaki, M. Tomonaga, S. Kamihara, Fas gene mutation in the progression of adult T cell leukemia, J. Exp. Med. 189 (1999) 1063–1071.
[25] N. Fukushima, Y. Nishiura, T. Nakamura, Y. Yamada, S. Kohno, K. Eguchi, Involvement of p38 MAPK signaling pathway in IFN-g and HTLV-I expression in patients with HTLV-I-associated myelopathy/tropical spastic paraparesis, J. Neuroimmunol. 159 (2005) 196–202.
[26] S. Pascolo, N. Bervas, J.M. Ure, A.G. Smith, F.A. Lemonnier, B. Perarnau, HLA-A2.1-restricted education and cytolytic activity of CD8(+) T lymphocytes from b2 microglobulin (b2m) HLA-A2.1 monochain transgenic H-2Db b2m double knockout mice, J. Exp. Med. 185 (1997) 2043–2051.
[27] T. Okazaki, C.D. Pendleton, F. Lemonnier, J.A. Berzofsky, Epitope-enhanced conserved HIV-1 peptide protects HLA-A2-transgenic mice against virus expressing HIV-1 antigen, J. Immunol. 171 (2003) 2548–2555.
[28] T. Okazaki, M. Terabe, A.T. Catanzaro, C.D. Pendleton, R. Yarchoan, J.A. Berzofsky, Possible therapeutic vaccine strategy against human immunodeficiency virus escape from reverse transcriptase inhibitors studied in HLA-A2 transgenic mice, J. Virol. 80 (2006) 10645–10651.
[29] A. Maeda, T. Okazaki, M. Inoue, T. Kitazono, M. Yamasaki, F.A. Lemonnier, S. Ozaki, Immunosuppressive effect of angiotensin receptor blocker on stimulation of mice CTLs by angiotensin II, Int. Immunopharmacol. 9 (2009) 1183–1188.
[30] B. Lee, Y. Tanaka, H. Tozawa, Monoclonal antibody defining tax protein of human T-cell leukemia virus type-I, Tohoku J. Exp. Med. 157 (1989) 1–11.
[31] Y. Yamano, N. Araya, T. Sato, A. Utsunomiya, K. Azakami, D. Hasegawa, T. Izumi, H. Fujita, S. Aratani, N. Yagishita, R. Fujii, K. Nishioka, S. Jacobson, T. Nakajima, Abnormally high levels of virus-infected IFN-g+ CCR4+ CD4+ CD25+ T cells in a retrovirus-associated neuroinflammatory disorder, PLoS ONE 4 (2009) e6517.
[32] F. Gotch, J. Rothbard, K. Howland, A. Townsend, A. McMichael, Cytotoxic T lymphocytes recognize a fragment of influenza virus matrix protein in association with HLA-A2, Nature 326 (1987) 881–882.
[33] M.H. Newberg, J.P. Ridge, D.R. Vining, R.D. Salter, V.H. Engelhard, Species specificity in the interaction of CD8 with the a3 domain of MHC class I molecules, J. Immunol. 149 (1992) 136–142.
[34] M.A. Alexander-Miller, G.R. Leggatt, J.A. Berzofsky, Selective expansion of high- or low-avidity cytotoxic T lymphocytes and efficacy for adoptive immunotherapy, Proc. Natl. Acad. Sci. USA 93 (1996) 4102–4107.
[35] C. Sedlik, G. Dadaglio, M.F. Saron, E. Deriaud, M. Rojas, S.I. Casal, C. Leclerc, In vivo induction of a high-avidity, high-frequency cytotoxic T-lymphocyte response is associated with antiviral protective immunity, J. Virol. 74 (2000) 5769–5775.
[36] V. Dutoit, V. Rubio-Godoy, P.Y. Dietrich, A.L. Quiqueres, V. Svhnuriger, D. Rimoldi, D. Lienard, D. Speiser, P. Guillaume, P. Batard, J.C. Cerottini, P. Romero, D. Valmori, Heterogeneous T-cell response to MAGE-A10(254–262): high avidity-specific cytolytic T lymphocytes show superior antitumor activity, Cancer Res. 61 (2001) 5850–5856.
[37] C. Yee, P.A. Savage, P.P. Lee, M.M. Davis, P.D. Greenberg, Isolation of high avidity melanoma-reactive CTL from heterogeneous populations using peptide-MHC tetramers, J. Immunol. 162 (1999) 2227–2234.
[38] H.J. Zeh III, D. Perry-Lalley, M.E. Dudley, S.A. Rosenberg, J.C. Yang, High avidity CTLs for two self-antigens demonstrate superior in vitro and in vivo antitumor efficacy, J. Immunol. 162 (1999) 989–994.
[39] C.R. Bangham, CTL quality and the control of human retroviral infections, Eur. J. Immunol. 39 (2009) 1700–1712.
[40] H. Konishi, N. Kobayashi, M. Hatanaka, Defective human T-cell leukemia virus in adult T-cell leukemia patients, Mol. Biol. Med. 2 (1984) 273–283.
[41] T. Kinoshita, M. Shimoyama, K. Tobinai, M. Ito, S. Ito, S. Ikeda, K. Tajima, K. Shimotohno, T. Sugimura, Detection of mRNA for the tax1/rex1 gene of human T-cell leukemia virus type I in fresh peripheral blood mononuclear cells of adult T-cell leukemia patients and viral carriers by using the polymerase chain reaction, Proc. Natl. Acad. Sci. USA 86 (1989) 5620–5624.
[42] T. Uchiyama, Human T cell leukemia virus type I (HTLV-I) and human diseases, Annu. Rev. Immunol. 15 (1997) 15–37.
[43] E.M. Choi, J.L. Chen, L. Wooldridge, M. Salio, A. Lissina, N. Lissin, I.F. Hermans, J.D. Silk, F. Milza, M.J. Palmowski, P.R. Dumbar, B.K. Jacobson, A.K. Sewell, V. Cerundolo, High avidity antigen-specific CTL identified by CD8-independent tetramer staining, J. Immunol. 171 (2003) 5116–5123.
[44] M. Kannagi, H. Shida, H. Igarashi, K. Kuruma, H. Murai, Y. Aono, I. Maruyama, M. Osame, T. Hattori, H. Inoko, Target epitope in the Tax protein of human T-cell leukemia virus type I recognized by class I major histocompatibility complex-restricted cytotoxic T cells, J. Virol. 66 (1992) 2928–2933.
[45] C. Govers, Z. Sebestyen, M. Coccoris, R.A. Willemsen, R. Debets, T cell receptor gene therapy: strategies for optimizing transgenic TCR pairing, Trends Mol. Med. 16 (2010) 77–87.

ARTHRITIS & RHEUMATISM
Vol. 63, No. 12, December 2011, pp 3833–3842
DOI 10.1002/art.30617

Overexpression of *SPACIA1/SAAL1*, a Newly Identified Gene That Is Involved in Synoviocyte Proliferation, Accelerates the Progression of Synovitis in Mice and Humans

Tomoo Sato,[1] Ryoji Fujii,[1] Koji Konomi,[2] Naoko Yagishita,[1] Satoko Aratani,[3] Natsumi Araya,[1] Hiroyuki Aono,[2] Kazuo Yudoh,[1] Noboru Suzuki,[1] Moroe Beppu,[1] Yoshihisa Yamano,[1] Kusuki Nishioka,[4] and Toshihiro Nakajima[5]

Objective. **To identify novel genes associated with dysregulated proliferation of activated synovial fibroblasts, which are involved in arthritic joint destruction.**

Methods. **We performed transcriptome analysis to identify genes that were up-regulated in the foot joints of mice with collagen-induced arthritis (CIA). The effect of candidate genes on proliferation of synovial fibroblasts was screened using antisense oligodeoxynucleotides and small interfering RNAs (siRNAs). We characterized the expression and function of a novel gene, synoviocyte proliferation–associated in collagen-induced arthritis 1 (*SPACIA1*)/serum amyloid A–like 1 (*SAAL1*) using antibodies and siRNA and established transgenic mice to examine the effect of SPACIA1/SAAL1 overexpression in CIA.**

Results. **Human and mouse *SPACIA1/SAAL1* encoded 474 amino acid proteins that shared 80% homology. SPACIA1/SAAL1 was primarily expressed in the nucleus of rheumatoid arthritis (RA) synovial fibroblasts and was highly expressed in the hyperplastic lining of inflamed synovium. In addition, its expression level in RA- or osteoarthritis (OA)–affected synovial tissue was positively correlated with the thickness of the synovial lining. Furthermore, *SPACIA1/SAAL1* siRNA inhibited the proliferation of synovial fibroblasts, especially tumor necrosis factor α–induced synovial fibroblasts, by blocking entry into the S phase without inducing apoptosis. Finally, transgenic mice overexpressing *SPACIA1/SAAL1* exhibited early onset and rapid progression of CIA.**

Conclusion. **These results suggest that SPACIA1/SAAL1 is necessary for abnormal proliferation of synovial fibroblasts and its overexpression is associated with the progression of synovitis in mice and humans. Thus, therapy targeting SPACIA1/SAAL1 might have potential as an inhibitor of synovial proliferation in RA and/or OA.**

Synovitis is a common characteristic of rheumatoid arthritis (RA) and knee osteoarthritis (OA). The major pathologic features of synovitis are hyperplasia of the synovial lining, inflammatory cell infiltration, and

Supported by Santen Pharmaceutical; the National Institute of Biomedical Innovation (Grant-in-Aid for Scientific Research); the Japanese Ministry of Education, Culture, Sports, Science, and Technology; the Japanese Ministry of Health, Labor, and Welfare; the Kato Memorial Trust for Nanbyo Research; the Japan Medical Association; the Nagao Memorial Foundation; the Kanae Foundation for Life and Socio-Medical Science; the Japan Research Foundation for Clinical Pharmacology; the Kanagawa Nanbyo Foundation; the Kanagawa Academy of Science and Technology; the Japan College of Rheumatology; the Nakajima Foundation; the Osaka Foundation for Cancer Research; the Japan Society for the Promotion of Science; the New Energy and Industrial Technology Development Organization; the Mochida Memorial Foundation; the Kanagawa High-Technology Foundation; the Kanto Bureau of Economy, Trade, and Industry; the Mitsui Life Welfare Foundation; the Uehara Memorial Foundation; the Heiwa Nakajima Foundation; the Sagawa Foundation for Promotion of Cancer Research; the Tokyo Biochemical Research Foundation; the Naito Foundation; the Daiichi-Sankyo Foundation of Life Science; the Bureau of Social Welfare and Public Health; and the Takeda Science Foundation.

[1]Tomoo Sato, MD, PhD, Ryoji Fujii, PhD, Naoko Yagishita, MS, Natsumi Araya, PhD, Kazuo Yudoh, MD, PhD, Noboru Suzuki, MD, PhD, Moroe Beppu, MD, PhD, Yoshihisa Yamano, MD, PhD: St. Marianna University School of Medicine, Kawasaki, Japan; [2]Koji Konomi, PhD, Hiroyuki Aono, PhD: Santen Pharmaceutical, Osaka, Japan; [3]Satoko Aratani, PhD: Tokyo Medical University, Tokyo, Japan, and St. Marianna University School of Medicine, Kawasaki, Japan; [4]Kusuki Nishioka, MD, PhD: Tokyo Medical University, Tokyo, Japan; [5]Toshihiro Nakajima, MD, PhD: Tokyo Medical University, Tokyo, Japan, Misato Marine Hospital, Kochi, Japan, and St. Marianna University School of Medicine, Kawasaki, Japan.

Address correspondence to Ryoji Fujii, PhD, Institute of Medical Science, St. Marianna University School of Medicine, 2-16-1 Sugao Miyamae-ku, Kawasaki 216-8512, Japan. E-mail: rfujii@marianna-u.ac.jp.

Submitted for publication November 21, 2010; accepted in revised form August 9, 2011.

high stromal cell density (1). Activated synovial fibroblasts, which are a major component of synovial lining hyperplasia, are important in the pathogenesis of synovitis because they secrete cytokines and chemokines, leading to the exacerbation of inflammation. They also produce matrix metalloproteinases and cathepsins, which destroy bone and cartilage (2). As a result, the activated synovial fibroblasts form pannus, a type of granulation tissue that erodes the joint (3). Therefore, reducing the number of activated synovial fibroblasts is a promising therapeutic strategy for arthritis. For example, adenoviral gene transfer of cyclin-dependent kinase inhibitors, such as p16 or p21, inhibits synovial cell proliferation and has demonstrated high therapeutic efficacy in animal models of RA (4,5). Similarly, intraarticular injection of anti-Fas IgM monoclonal antibodies induces apoptosis in synoviocytes and infiltrating lymphocytes, which leads to improvement of RA (6).

Although these findings suggest that synoviocyte proliferation is important in the pathogenesis of RA, the exact molecular mechanism of the disease is not known. To clarify the mechanism of the abnormal proliferation of synovial fibroblasts in RA, we used gene expression and functional analyses to seek novel genes that are involved in this process. Herein we describe a novel gene, synoviocyte proliferation–associated in collagen-induced arthritis 1 (*SPACIA1*)/serum amyloid A–like 1 (*SAAL1*), which was found to be up-regulated in the foot joints of mice with collagen-induced arthritis (CIA). Knockdown of this gene inhibited the proliferation of human RA synovial fibroblasts (RASFs) in vitro. Finally, we demonstrated that overexpression of *SPACIA1*/*SAAL1* is associated with the progression of synovitis in mice and humans.

MATERIALS AND METHODS

Ethical considerations. All human and animal experimental protocols in this study (nos. 443 and 31M0912T2, respectively) were approved by the Ethics Review Committee of St. Marianna University School of Medicine. Written informed consent was obtained from all patients prior to collection of joint tissue samples.

Animals. Male DBA/1J mice were purchased from Japan SLC. DBA/1J mice and transgenic mice were raised under conventional conditions at our facilities. Tap water and food were provided ad libitum.

Induction and assessment of CIA. For the microarray experiments, 10 DBA/1J mice (7–8 weeks old) were immunized twice with 100 μg bovine type II collagen (CII), as described previously (7). Seven days after the second injection of CII, collagen-injected mice and control mice were killed and foot joints were removed from their forepaws.

To induce CIA in *SPACIA1*-overexpressing mice, CII was administered as described above, except that the amount of CII administered in the second injection was reduced to 50 μg. Subsequently, the mice were assessed 3 times per week, and an arthritis score was assigned based on the grading system described by Hughes et al (8). In addition, blood samples were collected from the tail vein once per week to measure anti-CII antibody titers. Forty-two days after the first injection, the mice were weighed and killed, and samples of their blood, spleen, and knee joints were collected.

DNA microarray. Total RNA was extracted and pooled from the foot joint samples from the mice with CIA and from the control mice. Messenger RNA (mRNA) was isolated using the PolyATtract mRNA Isolation System (Promega). Double-stranded complementary DNA (cDNA) was synthesized from 1 μg mRNA, followed by preparation of biotinylated complementary RNA (cRNA) with the BioArray HighYield RNA Transcript Labeling Kit (Affymetrix). Biotin-labeled cRNA, which was fragmented according to the Affymetrix procedure, was hybridized to Murine Genome U74v2 microarrays. Subsequently, these microarrays were stained with streptavidin–phycoerythrin and scanned with a GeneArray scanner. The intensity data from each array were normalized using Microarray Suite version 5.0 software. To determine the $\log_2$ ratio of signal intensities, we compared the normalized data from mice with CIA to the data from the control group, using Data Mining Tool version 3.0 software. The microarrays, scanner, and software sets were all obtained from Affymetrix, and all of the annotation data for the identified probe sets were obtained from the NetAffx Analysis Center (http://www.affymetrix.com/analysis/index.affx).

Design and use of antisense oligodeoxynucleotides (ODNs) and small interfering RNAs (siRNAs) in cell proliferation assays. To screen candidate genes, we designed antisense phosphorothioated ODNs near the start codon, using Oligo software (Molecular Biology Insights). We also designed siRNAs, using the design program on the Takara Bio web site (http://www.takara-bio.co.jp/rnai/intro.htm). The ODNs and siRNAs were chemically synthesized at Hokkaido System Science. Their sequences are shown in Supplementary Tables 1 and 2 (available on the *Arthritis & Rheumatism* web site at http://onlinelibrary.wiley.com/journal/10.1002/(ISSN)1529-0131).

RASFs were isolated and cultured as described previously (9). Twenty-four hours before transfection, the cells were trypsinized, seeded on a 24-well plate, and cultured overnight. To determine the effect of antisense ODNs and siRNAs on the proliferation of RASFs, we transfected 100 n*M* antisense ODN or 100 n*M* siRNA into the cells with Oligofectamine (Invitrogen) and then cultured the cells for 66 hours or 96 hours, respectively. Subsequently, we used the Cell Counting Kit-8 assay (Dojindo) to determine the relative number of viable cells.

Similarly, to determine the effect of *SPACIA1* siRNA on RASF proliferation induced by serum or tumor necrosis factor α (TNFα), we used *SAAL1* (also known as *SPACIA1*) siRNA, c-*fos* siRNA, and negative control siRNA (On-Target plus SMARTpool; Dharmacon). RASFs were then trypsinized and seeded in 48-well plates. After 18 hours, 33 n*M* siRNA was transfected into the cells with Lipofectamine 2000 (Invitrogen) in Opti-MEM medium. Four hours later, the culture medium

was changed to Dulbecco's modified Eagle's medium supplemented with 10% fetal bovine serum (FBS) or 1% FBS and 5 ng/ml TNFα. Finally, 96 hours after transfection, we determined the relative number of viable RASFs, using the Cell Counting Kit-8 assay.

Cloning and expression of human SPACIA1 and preparation of anti-SPACIA1 antibodies. We designed the following polymerase chain reaction (PCR) primers on the basis of the sequence of human *SAAL1*, which is identical to *SPACIA1* (GenBank Refseq NM_138421; http://www.ncbi.nlm.nih.gov/genbank/): for the first PCR, hSPACIA1+ 5′-AAAGTCATGGACCGCAAC-3′, hSPACIA1− 5′-CCAATTCAGGTTTTAAGTCTGAAC-3′; for the second PCR, hSPACIA1+/*Not* I 5′-ATATGCGGCCGCCGATGGACCGCAACCCCTCG-3′, hSPACIA1−/*Xho* I 5′-TCACTCGAGGTTTTAAGTCTGAACCTTC-3′. Human RASF cDNA was used as a template for PCR. The product was cloned into a pcDNA3-FLAG vector, which was constructed by inserting the FLAG sequence into pcDNA3 (Invitrogen). To create a GST-SPACIA1 fusion protein, the *SPACIA1* gene was subcloned into a pGEX-6P vector (GE Healthcare) and then transformed into *Escherichia coli* BL21 cells. The transfected cells were cultured for 4 hours at 30°C in the presence of 0.1 m*M* isopropyl β-D-1-thiogalactopyranoside. Subsequently, the cells were sonicated, and the recombinant human SPACIA1 protein was purified from the lysate with a glutathione Sepharose 4B column (GE Healthcare) and PreScission protease cleavage. Finally, the purified human SPACIA1 protein was used as an antigen to generate polyclonal antibodies and monoclonal antibodies (pAb and mAb, respectively), using standard methods as previously described (10,11).

Western blotting. Synovial fibroblasts from patients with RA and synovial tissue from patients with OA and RA were lysed in lysis buffer (20 m*M* Tris [pH 7.5], 150 m*M* NaCl, 0.5% Nonidet P40, 1 m*M* EDTA, 1 m*M* dithiothreitol, 5 m*M* NaF, 0.2 m*M* Na_3VO_4, and protease inhibitors). Then whole cell lysates (10 μg) or tissue lysates (20 μg) were electrophoresed on 10% sodium dodecyl sulfate polyacrylamide gels and transferred onto activated Immobilon-P polyvinylidene fluoride membranes (Millipore) using a wet transfer method. After blocking with 5% nonfat dry milk in phosphate buffered saline (PBS), the membranes were incubated with anti-human SPACIA1 mAb (clone 1Ac; 1:500 dilution), followed by incubation with horseradish peroxidase (HRP)–labeled anti-mouse IgG antibody (1:20,000 dilution; The Binding Site) for 1 hour at room temperature, and detection with Immobilon Western Chemiluminescent HRP Substrate (Millipore). The signal intensities of the bands specific for SPACIA1 were quantified using ImageJ software (National Institutes of Health; http://rsbweb.nih.gov/ij/). To investigate the expression of SPACIA1 in various human tissues, we used a human multiple tissue blot (Calbiochem). The detection method was the same as described above, except the primary antibody was anti-human SPACIA1 pAb (1:8,000 dilution) and the secondary antibody was HRP-labeled anti-rabbit IgG antibody (1:20,000 dilution).

Immunocytochemistry. To determine the intracellular localization of SPACIA1 in RASFs, we performed immunofluorescence staining as previously described (12). Anti-human SPACIA1 mAb (clone 1Ac) and normal mouse IgG were used as the primary antibody and negative control, respectively. The secondary antibody was a rhodamine-conjugated anti-mouse IgG antibody (Millipore). Nuclei were stained with DAPI.

Immunohistochemistry. Human synovial tissue specimens and mouse knee joints were fixed in 10% formalin and then embedded in paraffin. To retrieve antigens, deparaffinized tissue sections (5 μm thick) were microwaved for 5 minutes and soaked in 1 m*M* EDTA solution (pH 8.0) for 40 minutes at 90°C. After blocking of endogenous peroxidase activity for 10 minutes in 3% methanol, the sections were incubated with anti-human SPACIA1 pAb (1.5 μg/ml), normal rabbit IgG (1.5 μg/ml), anti-CD14 mAb (1:150 dilution; Leica), anti-CD163 mAb (1:150 dilution; Leica), or normal mouse IgG (1 μg/ml) for 30 minutes at room temperature. Subsequently, the sections were rinsed and visualized by immunoperoxidase staining with the Vectastain ABC-PO kit (Vector) and 3,3′-diaminobenzidine tetrahydrochloride substrate. Mayer's hematoxylin was used as a counterstain. Normal rabbit IgG and normal mouse IgG were used as negative controls.

Cell cycle phase analysis. To analyze the effect of *SPACIA1* siRNA on the cell cycle of RASFs, we used *SPACIA1* siRNA and mock siRNA. The target sequences were as follows: human SPACIA1 3′-untranslated region siRNA 5′-GAAUUACUUCUGUACAAGAA-3′, mock siRNA (negative control) 5′-UAAGGCUAUGAAGAGAUAC-3′. Ninety-six hours after transfection of siRNA into RASFs, the cells were harvested, washed, and suspended in PBS with 0.1% Triton X-100. The suspension was filtered through nylon mesh to remove aggregates. Subsequently, RNase and propidium iodide were added to the suspension, which was analyzed on a FACSCalibur flow cytometer (BD Biosciences). The results were analyzed using FlowJo software (Tree Star).

Annexin V–based apoptosis assay. To evaluate apoptotic cells, we used the same siRNAs that were used for the cell cycle analysis and analyzed RASFs 96 hours after transfection. RASFs that were treated with 10 μ*M* staurosporine for 3 hours and cultured for 12 hours were used as a positive control. Staurosporine-treated or siRNA-transfected RASFs were stained with fluorescein isothiocyanate (FITC)–labeled annexin V (MBL) using a previously described immunofluorescence staining procedure (12), and the percentage of annexin V–positive RASFs in 3 microscopic fields (200×) was calculated.

Bromodeoxyuridine (BrdU) incorporation assay. For measurement of BrdU incorporation, we used *SPACIA1* siRNA, negative control siRNA, and *PCNA* siRNA (proliferating cell nuclear antigen) (On-Target plus SMARTpool). RASFs were trypsinized and then seeded on a 6-well plate (1.4×10^5 cells/well). After 18 hours, 33 n*M* siRNA was transfected into the cells with Lipofectamine 2000. Twenty-four hours later, 10 μ*M* aphidicolin was added to the culture media for 24 hours to synchronize the cells at the G_1 phase. Then the aphidicolin was removed and DNA synthesis was determined by measurement of BrdU incorporation for 8 hours. Subsequently, the cells were fixed, permeabilized, treated with DNase I, and stained for 1 hour with an FITC-labeled anti-BrdU antibody (BD Biosciences). Fluorescence intensity was measured with a Cellomics ArrayScan VTI HCS reader (Thermo Fisher Scientific).

Generation of *SPACIA1*-overexpressing mice. On the basis of the sequence of mouse *SAAL1* (GenBank Refseq NM_030233), we designed the following primers: for the first

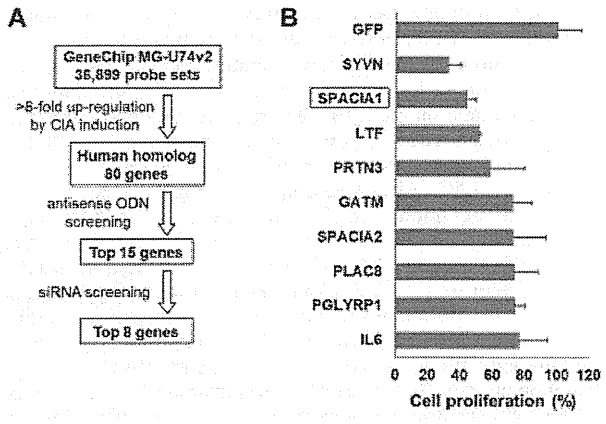

Figure 1. Identification of *SPACIA1* by whole-genome microarray analysis and functional screening. **A**, Flow chart of the procedure that was used to select 8 genes from >36,000 mouse transcripts. Eighty genes were up-regulated >8-fold in the foot joints of mice with collagen-induced arthritis (CIA). Among these genes, 15 genes that inhibited the proliferation of human rheumatoid arthritis synovial fibroblasts (RASFs) were identified with antisense oligodeoxynucleotides (ODNs). Finally, 8 candidate genes were isolated using small interfering RNAs (siRNAs) that were targeted against these 15 genes. **B**, Rate of proliferation of RASFs that were transfected with siRNA targeted against the candidate genes. The results are expressed as the percentage of the proliferation rate of RASFs that were transfected with green fluorescence protein (GFP) siRNA (negative control). Small interfering RNA against synoviolin (*SYVN*), an E3 ubiquitin ligase that we previously identified as a pathogenic factor in arthropathy (7), was used as a positive control. All experiments were performed in triplicate. Values are the mean ± SD.

PCR, mSPACIA1+ 5′-CATCGGCATGGATCGAAAC–3′, mSPACIA1− 5′-ATGCCAACTTCGAACCATAG-3′; for the second PCR, mSPACIA1+/*Mun* I 5′-ATACAATTGATGGATCGAAACCCGTCTC-3′, mSPACIA1−/*Xho* I 5′-TAACTCGAGTTAAGTCTGTGCCTTCAC-3′. PCR was performed with a mouse embryo (17th day of gestation) cDNA as a template. The PCR product was cloned into the pcDNA3-FLAG vector, and the FLAG-tagged mouse *SPACIA1* gene was subcloned into the mammalian expression vector pJC13-1 (a kind gift from Dr. Suming Huang, University of Florida, Gainesville) with a CAG promoter and β-globin insulators (13). The linearized FLAG-tagged mouse SPACIA1 pJC13-1 expression vector was injected into the pronucleus of fertilized eggs from C57BL/6 mice (Macrogen). To confirm the overexpression of mouse *SPACIA1*, genomic DNA and protein were extracted from tails and used for PCR and Western blotting analyses, respectively. Finally, the *SPACIA1*-overexpressing mice were backcrossed onto the DBA/1J strain for 7 generations.

Histopathologic examination. Human synovial tissue specimens were obtained from patients with RA (n = 9) or OA (n = 9) and processed as described previously (14). Synovitis was scored on a 0–3 scale using the grading system of Krenn et al (1).

Mouse knee joints were removed 42 days after CIA induction, fixed in 10% formalin, and embedded in paraffin. Deparaffinized tissue sections (5 μm thick) were stained with hematoxylin and eosin. The sections were scored on a scale of 0–4 under blinded conditions, according to the degree of hyperplasia in the synovial lining, mononuclear cell infiltration, and pannus formation, as described previously (15).

Statistical analysis. Fisher's exact test was used to analyze the correlation between expression levels of SPACIA1 and pathologic features of synovitis. The significance of RASF proliferation was analyzed by one-way analysis of variance and Tukey's post hoc test. The chi-square test (or Fisher's exact test) was used to compare the incidence of arthritis between transgenic and wild-type mice. Arthritis scores and histopathologic scores in transgenic and wild-type mice were compared by Mann-Whitney U test. All other statistical analyses were performed using Student's unpaired *t*-test. *P* values less than 0.05 were considered significant.

RESULTS

Identification of novel genes associated with synoviocyte proliferation. In the transcriptome of the foot joints of mice with CIA, we detected 80 genes (among ~36,000 mRNA probes) that were up-regulated >8-fold compared with those of healthy control mice (Figure 1A). By transfecting human RASFs with antisense ODNs specific for the human homologs of these 80

Figure 2. Amino acid sequence alignment of mouse and human *SPACIA1*. The alignment was generated using the ClustalW2 multiple sequence alignment program (http://www.ebi.ac.uk/Tools/clustalw2/). Identical residues are marked with asterisks. Colons and periods indicate conserved substitutions and semiconserved substitutions, respectively. Shaded regions indicate armadillo repeats (InterPro accession no. IPR016024). Boxed amino acids indicate phosphorylation sites.

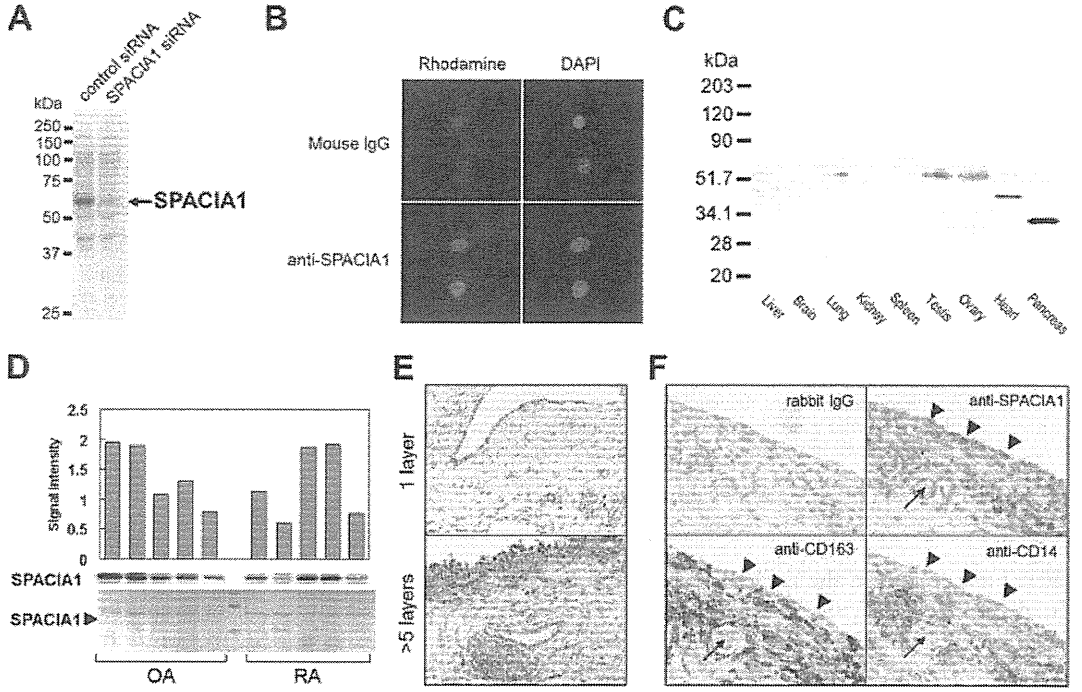

Figure 3. Expression analysis of SPACIA1 in human tissue. **A**, Western blotting of RASFs that were transfected with control or *SPACIA1* siRNA; an anti-SPACIA1 monoclonal antibody (mAb) was used for detection. **B**, Subcellular localization of SPACIA1 in RASFs. Immunofluorescence staining was performed with an anti-SPACIA1 mAb and normal mouse IgG. The images are representative of 3 separate experiments. **C**, Western blotting of various human tissues with an anti-SPACIA1 polyclonal antibody. **D**, Comparison of SPACIA1 expression levels in osteoarthritis (OA) and RA synovial tissue, by Western blotting. The membrane was stained with ponceau S to ensure equal protein loading in all lanes. The intensity of the SPACIA1-specific bands was quantified by densitometry. Another set of Western blots also showed no significant differences between RA and OA (data not shown). **E**, Expression of SPACIA1 in human synovium with or without hyperplasia of the synovial lining. SPACIA1-positive cells are brown. The images are representative of the results obtained in experiments with specimens from 5 different patients with RA or OA. Original magnification × 100. **F**, Localization of SPACIA1, CD163, and CD14 in serial sections of RA synovial membrane. **Arrowheads** show SPACIA1-positive, CD163-negative, and CD14-negative cells. **Arrows** show a capillary blood vessel. Original magnification × 200. See Figure 1 for other definitions.

genes (see Supplementary Table 1, available at http://onlinelibrary.wiley.com/journal/10.1002/(ISSN)1529-0131), we identified the top 15 genes ranked by their proliferative inhibition rate. Subsequently, by using siRNA against these genes (Supplementary Table 2 http://onlinelibrary.wiley.com/journal/10.1002/(ISSN)1529-0131), we reduced the number of genes associated with synoviocyte proliferation to 8 candidates (Figure 1). Among them, there were 2 genes with unknown functions. We named these genes synoviocyte proliferation–associated in collagen-induced arthritis 1 (*SPACIA1*) (GenBank accession no. AB489136 [human] and AB489137 [mouse]) and *SPACIA2* (GenBank accession no. AB541014 [human isoform 1], AB541015 [human isoform 2], and AB541013 [mouse]). The proliferation of RASFs was most strongly inhibited by *SPACIA1* siRNA, followed by lactotransferrin (*LTF*), proteinase 3 (*PRTN3*), glycine amidinotransferase (*GATM*), *SPACIA2*, placenta-specific gene 8 (*PLAC8*), peptidoglycan recognition protein 1 (*PGLYRP1*), and interleukin 6 (*IL6*). Therefore, we focused upon the role of *SPACIA1*.

Characterization of human and mouse *SPACIA1*. According to the NCBI nucleotide database (http://www.ncbi.nlm.nih.gov/nuccore), *SPACIA1* is identical to serum amyloid A–like 1 (*SAAL1*). The human and mouse *SPACIA1/SAAL1* genes are localized to chromosomes 11p15.1 and 7B4, respectively. These loci contain a gene cluster of the serum amyloid A (SAA) superfamily, which includes *SAA1*, *SAA2*, *SAA3*, and *SAA4* (16). The human and mouse SPACIA1/SAAL1 proteins are

Table 1. Correlation between expression level of SPACIA1 and pathologic features of synovitis in patients with RA or OA*

Feature	Low SPACIA1 expression, no. of patients	High SPACIA1 expression, no. of patients	P†
Synovial lining thickness			
Score 0–1 (≤4 layers)	9 (5 RA, 4 OA)	2 (0 RA, 2 OA)	
Score 2–3 (>4 layers)	0	7 (4 RA, 3 OA)	0.0011
Stromal cell density			
Score 0–1 (normal–mild)	8 (4 RA, 4 OA)	6 (1 RA, 5 OA)	
Score 2–3 (moderate–severe)	1 (1 RA, 0 OA)	3 (3 RA, 0 OA)	0.2882
Inflammatory cell infiltration			
Score 0–1 (normal–mild)	5 (2 RA, 3 OA)	2 (0 RA, 2 OA)	
Score 2–3 (moderate–severe)	4 (3 RA, 1 OA)	7 (4 RA, 3 OA)	0.1674

* Synovial tissue samples from 9 patients with rheumatoid arthritis (RA) and 9 patients with osteoarthritis (OA) were classified as having high or low expression of SPACIA1 based on the intensity of SPACIA1-specific bands shown on Western blotting. Synovial lining thickness, stromal cell density, and inflammatory cell infiltration were scored according to the synovitis grading system described by Krenn et al (1).

† Versus score of 0–1, by Fisher's exact test.

82% and 80% homologous at the nucleotide and amino acid levels, respectively (Figure 2). Furthermore, the NCBI HomoloGene database (http://www.ncbi.nlm.nih.gov/homologene) indicates that the sequence of the *SPACIA1/SAAL1* gene (unique identifier no. 34706) is conserved from zebrafish to humans. Although SPACIA/SAAL1 does not have any signal peptides, transmembrane domains, classic nuclear localization signals, or nuclear export signals, the InterPro database (http://www.ebi.ac.uk/interpro/) indicates that it has an armadillo-type motif (InterPro accession no. IPR016024) between amino acids 82 and 211 (Figure 2). In addition, previous proteomic studies showed that human and mouse SPACIA1/SAAL1 are phosphoproteins (Figure 2) .

The SAA protein family includes acute-phase proteins that are secreted in response to inflammation (19). Two members of this family, SAA1 and SAA2, are precursors of amyloid A, which causes amyloidosis secondary to RA (20). Thus, SAA plays an important role in inflammatory conditions, such as RA. However, the amino acid sequence of *SPACIA1* was not very similar to that of *SAA*; *SPACIA1* and *SAA1* are only 27% homologous. Moreover, unlike SAA proteins, which have a signal peptide and a conserved SAA domain, human and mouse SPACIA1/SAAL1 do not have either of these characteristics. As a result, we refer to SPACIA1/SAAL1 below as SPACIA1.

Expression analysis of human SPACIA1. Human SPACIA1 is a 55-kd protein that is expressed in RASFs (Figure 3A) and is predominantly localized to the nuclei (Figure 3B). In addition, SPACIA1 was strongly expressed in the testis and ovary, but only weakly expressed in the lung, spleen, and heart (Figure 3C). A 40-kd protein in the heart and a 30-kd protein in the pancreas were also detected with the anti-SPACIA1 pAb, but these results may have been due to nonspecific binding. Although SPACIA1 was also expressed abundantly in the synovial tissue of patients with RA or OA (Figure 3D), we did not observe any specific pattern in the expression levels of SPACIA1 in RA or OA synovial tissue. However, the expression level of SPACIA1 was significantly correlated with the thickness of the synovial lining, but not with the density of stromal cells or inflammatory cell infiltrates (Table 1). As expected from these results, SPACIA1 was strongly expressed in the hyperplastic synovial lining and moderately expressed in synovial stromal cells, endothelial cells, and plasma cells (Figure 3E). Interestingly, the localization of SPACIA1-positive cells was the opposite of that of CD14- or CD163-positive cells, which are considered to be synovial macrophages (Figure 3F).

Antiproliferative effect of *SPACIA1* siRNA in synovial fibroblasts. As shown in Figure 4A, *SPACIA1* siRNA inhibited the proliferation of RASFs that were stimulated with 10% FBS. However, this effect was significantly weaker than that of the positive control, *c-fos* siRNA, which strongly inhibits the proliferation of RASFs (21). On the other hand, the inhibitory effect of *SPACIA1* siRNA on the proliferation of RASFs that were stimulated with TNFα was comparable to that of *c-fos* siRNA (Figure 4B). Furthermore, flow cytometric analysis demonstrated that transfection of *SPACIA1* siRNA into RASFs increased the number of cells in the

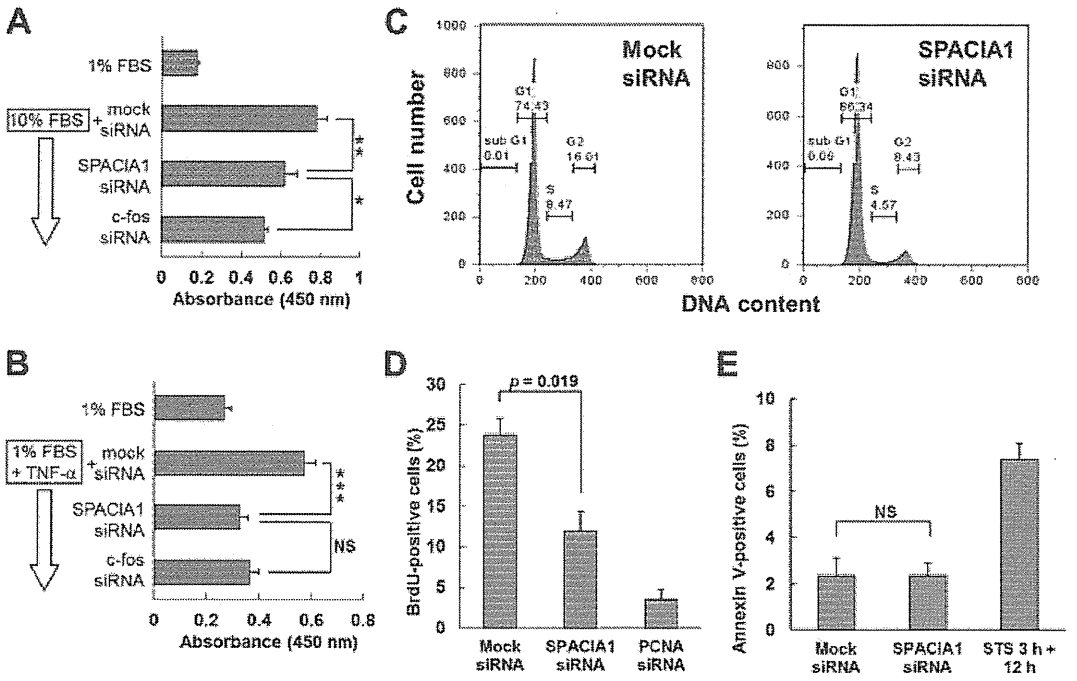

Figure 4. Antiproliferative effect of *SPACIA1* siRNA on RASFs by partial inhibition of entry into the S phase. **A** and **B**, *SPACIA1* siRNA suppressed the proliferation of RASFs in response to 10% fetal bovine serum (FBS) (**A**) or 5 ng/ml tumor necrosis factor α (TNFα) (**B**); c-*fos* siRNA was used as a positive control. Data are representative of 5 separate experiments in **A** and 3 separate experiments in **B**. Values are the mean ± SD. * = $P < 0.05$; ** = $P < 0.01$; *** = $P < 0.001$. NS = not significant. **C**, After culture of RASFs in medium supplemented with 10% FBS, *SPACIA1* siRNA reduced the number of RASFs in the S and G_2/M phase, compared with mock siRNA. Representative histograms from 3 different experiments are shown. **D**, After culture of RASFs in medium supplemented with 10% FBS, *SPACIA1* siRNA significantly inhibited the entry of RASFs into the S phase in a bromodeoxyuridine (BrdU) incorporation assay, compared with mock siRNA. *PCNA* siRNA was used as a positive control. Values are the mean ± SD (n = 3 experiments). **E**, After culture of RASFs in medium supplemented with 10% FBS, *SPACIA1* siRNA did not induce apoptosis in an annexin V apoptosis assay. RASFs that were treated with staurosporine (STS) for 3 hours and cultured for 12 hours were used as a positive control. Values are the mean ± SD. Experiments in **A, B, D,** and **E** were performed in triplicate. See Figure 1 for other definitions.

G_0/G_1 phase and reduced the number of cells in the S and G_2/M phase compared with mock siRNA transfection (Figure 4C). A BrdU incorporation assay showed that the percentage of BrdU-positive RASFs was 24%, 12%, and 4% after transfection with mock, *SPACIA1*, or *PCNA* siRNA, respectively (Figure 4D). Moreover, the percentage of annexin V–positive RASFs was similar after transfection with *SPACIA1* and mock siRNA (Figure 4E).

Progression of CIA in transgenic mice overexpressing *SPACIA1*. A schematic representation of the mammalian expression construct that was used to create transgenic mice overexpressing *SPACIA1* is shown in Figure 5A. The overexpression of *SPACIA1* in the transgenic mice was confirmed by Western blotting (Figure 5B) and PCR (results not shown). These transgenic mice did not spontaneously develop arthritis or cancer. Since findings of a preliminary experiment suggested that *SPACIA1*-transgenic mice are more sensitive to CIA than wild-type mice, we reduced the amount of CII that was used to induce arthritis, to more easily detect the difference in their sensitivity to CIA. Despite this modification, the incidence of CIA in the transgenic mice increased significantly more rapidly than in the wild-type mice, particularly at 30–37 days after the first injection of collagen (Figure 5C). Furthermore, the arthritis score in the paws of transgenic mice with CIA was significantly higher than that of wild-type mice at 30–39 days after the first injection (Figure 5D), and the histopathologic scores of the knee joints of the transgenic mice were significantly higher than in the wild-type mice (Figure 5E). Finally, immunohistochemistry was

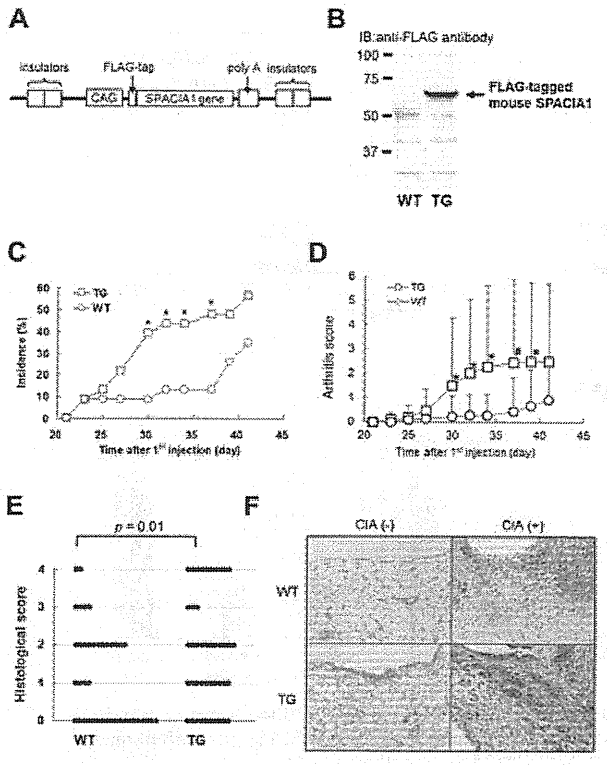

Figure 5. Early onset and rapid progression of collagen-induced arthritis (CIA) in transgenic (Tg) mice overexpressing *SPACIA1*. **A**, Schematic representation of the transgene for overexpression of mouse *SPACIA1*. **B**, Immunoblot (IB) analysis of lysates from tail tissue of wild-type (WT) and Tg mice, using an anti-FLAG antibody. **C**, Development of arthritis in 23 WT and 23 Tg mice after injection of bovine type II collagen (CII) on days 0 and 21. Arthritis incidence was significantly higher in Tg mice than in WT mice on days 30–37. * = $P < 0.05$ versus WT mice. **D**, Arthritis severity in 23 WT and 23 Tg mice after injection of CII on days 0 and 21. Arthritis scores were significantly higher in Tg mice than in WT mice on days 30–39. Values are the mean ± SD. * = $P < 0.05$; # = $P < 0.01$, versus WT mice. **E**, Histopathologic scores in the knee joints of 23 WT and 23 Tg mice after injection of CII on days 0 and 21. **F**, Expression of SPACIA1 protein in synovial tissue from the knee joints of WT and Tg mice with or without CIA. Original magnification × 100.

performed to examine the expression levels of SPACIA1 protein in the joints of the mice with CIA (Figure 5F). The number of SPACIA1-positive cells was markedly increased in the joints of both wild-type and transgenic mice with CIA.

DISCUSSION

In this study of ~36,000 mRNA transcripts, we identified a novel gene, *SPACIA1*, that is involved in the dysregulated proliferation of synovial fibroblasts in the foot joints of mice with CIA. However, since the forepaw tissue samples included not only synovium but also bone, cartilage, muscle, and tendon tissue, the transcriptome analysis was not specific for genes that are expressed in the synovium. To overcome this problem, we used human RASFs to screen the candidate genes that were identified from the transcriptome analysis. We found that SPACIA1 was expressed not only in cultured RASFs (Figure 3A and B) but also in the inflamed joints of mice and humans (Figures 3E and 5F). Notably, SPACIA1 was strongly expressed in synovial fibroblasts, and not in synovial macrophages, in the intimal layer of the synovial membrane of human RA patients (Figure 3F). Furthermore, its expression in human synovial tissue was not specific to RA, as was demonstrated by its expression in synovial tissue from patients with OA as well (Figure 3D). Similar to RA, synovitis commonly occurs in end-stage OA (22). In fact, 90% of joints from OA patients undergoing arthroplasty contain pannus-like tissue on the articular surface (23). As a result, SPACIA1 may be expressed at comparable levels in OA and RA synovia.

Transgenic mice overexpressing *SPACIA1* exhibited earlier onset and more rapid progression of CIA than wild-type mice (Figures 5C–E). In addition, the expression level of SPACIA1 was positively correlated with the thickness of the synovial lining in humans (Table 1). These results suggest that overexpression of SPACIA1 accelerates the progression of synovitis by promoting synovial cell proliferation. However, it is unlikely that SPACIA1 overexpression affected the immune system, because we did not observe any significant difference in the ratio of spleen weight to body weight between the wild-type and transgenic mice with CIA (data not shown). In addition, there were no significant differences in anti-CII antibody titers in serum from the wild-type and transgenic mice with CIA (data not shown). With regard to the use of transgenic mice overexpressing FLAG-tagged mouse SPACIA1, there is both a benefit and a limitation that should be considered. The benefit is that FLAG-tagged mouse SPACIA1 is easy to distinguish from endogenous mouse SPACIA1. The limitation is that we were not able to identify any potential side effects of the FLAG tag when we evaluated these transgenic mice. However, to minimize this potential effect, we confirmed that there are no significant domains in the N-terminal region of SPACIA1, e.g., a signal peptide.

Since *SPACIA1* knockdown inhibited synoviocyte proliferation, our results indicate that SPACIA1 should

be implicated in the abnormal proliferation of synovial fibroblasts in synovitis due to an antiapoptotic effect or stimulation of cell cycle progression. In this regard, although *SPACIA1* knockdown inhibited the entry of RASFs into the S phase (Figures 4C and D), it did not induce apoptosis in RASFs (Figure 4E). In addition, our ongoing studies indicate that *SPACIA1* knockdown halves the expression of the genes for cyclin E2 and cyclin-dependent kinase 2, which are involved in the progression of the cell cycle from G_1 to S (Sato T, et al: unpublished observations). Therefore, it is more likely that SPACIA1 regulates the progression of the cell cycle than that it regulates apoptosis in RASFs.

What is the possible mechanism of action of SPACIA1? When we screened the molecules that interact with SPACIA1 using a yeast 2-hybrid assay, most of the molecules obtained were transcription regulatory factors that are located in the nucleus (data not shown). This suggests that SPACIA1 might act as a transcriptional regulator by forming a complex with certain molecules in the nucleus. We next considered the setting in which SPACIA1 acts. Because serum contains a variety of growth factors and hormones, the addition of serum to the culture medium represents a general stimulation that leads to proliferation of cells, whereas administration of TNFα represents an inflammatory stimulation that induces cell proliferation. Since *SPACIA1* knockdown was more efficient at blocking TNFα-induced proliferation than serum-induced proliferation (Figures 4A and B), SPACIA1 might be especially involved in the inflammatory signaling pathways that induce the proliferation of RASFs. Based on our findings, we speculate that SPACIA1 may act downstream of inflammatory signaling and regulate the transcription of cell cycle–implicated genes, which then regulate the expression of cyclin E2 and cyclin-dependent kinase 2. However, further investigation is needed to clarify the precise mechanism of action of SPACIA1, e.g., whether it affects any of the major signaling pathways, including the NF-κB or JNK pathway.

Moreover, there is in vivo evidence that the effect of SPACIA1 on synoviocyte proliferation is limited to inflammatory conditions. The transgenic mice overexpressing *SPACIA1* did not spontaneously develop arthritis or cancer, and administration of a collagen emulsion was still required for induction of synoviocyte proliferation. Therefore, unlike typical anticancer drugs, an SPACIA1 inhibitor may be able to specifically suppress abnormal synoviocyte proliferation in inflammatory environments with relatively few side effects.

In conclusion, the overexpression of SPACIA1, a novel protein that is involved in the proliferation of synovial fibroblasts, is associated with the progression of synovitis in mice and humans. Consequently, SPACIA1 might be a potential therapeutic target for inhibiting synovial proliferation in RA and OA.

ACKNOWLEDGMENTS

We would like to thank N. Watanabe-Asakura, K. Takahashi, N. Yamamoto, A. Une, N. Furuya, S. Shinkawa, Y. Nakagawa, K. Suzuki, S. Asada, T. Sato-Mogi, H. Ogasawara, Y. Sato, Y. Urbanczyk, M. Yamanashi, and M. Ishikawa for excellent technical assistance.

AUTHOR CONTRIBUTIONS

All authors were involved in drafting the article or revising it critically for important intellectual content, and all authors approved the final version to be published. Dr. Fujii had full access to all of the data in the study and takes responsibility for the integrity of the data and the accuracy of the data analysis.

Study conception and design. Fujii, Konomi, Nishioka, Nakajima.
Acquisition of data. Sato, Fujii, Konomi, Yagishita, Aratani, Araya.
Analysis and interpretation of data. Sato, Fujii, Konomi, Yagishita, Aratani, Araya, Aono, Yudoh, Suzuki, Beppu, Yamano, Nishioka, Nakajima.

ROLE OF THE STUDY SPONSOR

Santen Pharmaceutical collaborated with St. Marianna University School of Medicine in this study. Employees of Santen Pharmaceutical contributed to the study design, data collection, data analysis, and writing of the manuscript; however, Santen Pharmaceutical was not involved in the decision to submit the manuscript for publication or in approval of the content of the submitted manuscript, and publication of the manuscript was not contingent upon the approval of Santen Pharmaceutical.

REFERENCES

1. Krenn V, Morawietz L, Burmester GR, Kinne RW, Mueller-Ladner U, Muller B, et al. Synovitis score: discrimination between chronic low-grade and high-grade synovitis. Histopathology 2006; 49:358–64.
2. Ritchlin C. Fibroblast biology: effector signals released by the synovial fibroblast in arthritis. Arthritis Res 2000;2:356–60.
3. Mueller-Ladner U, Gay R, Gay S. Structure and function of synoviocytes. In: Koopman W, editor. Arthritis and allied conditions: a textbook of rheumatology. 14th ed. Philadelphia: Lippincott Williams & Wilkins; 2001. p. 285–300.
4. Taniguchi K, Kohsaka H, Inoue N, Terada Y, Ito H, Hirokawa K, et al. Induction of the p16INK4a senescence gene as a new therapeutic strategy for the treatment of rheumatoid arthritis. Nat Med 1999;5:760–7.
5. Nasu K, Kohsaka H, Nonomura Y, Terada Y, Ito H, Hirokawa K, et al. Adenoviral transfer of cyclin-dependent kinase inhibitor genes suppresses collagen-induced arthritis in mice. J Immunol 2000;165:7246–52.
6. Appelboom T, Mann H, Senolt L, Suchy D, Nemec P, Rolova J, et al. Preliminary results of a phase I clinical trial of intra-articular administration of ARG098, a novel anti-Fas IgM mAb, in RA [abstract]. Arthritis Rheum 2009;60 Suppl:S156.

7. Amano T, Yamasaki S, Yagishita N, Tsuchimochi K, Shin H, Kawahara K, et al. Synoviolin/Hrd1, an E3 ubiquitin ligase, as a novel pathogenic factor for arthropathy. Genes Dev 2003;17: 2436–49.
8. Hughes C, Wolos JA, Giannini EH, Hirsch R. Induction of T helper cell hyporesponsiveness in an experimental model of autoimmunity by using nonmitogenic anti-CD3 monoclonal antibody. J Immunol 1994;153:3319–25.
9. Izumi T, Fujii R, Izumi T, Nakazawa M, Yagishita N, Tsuchimochi K, et al. Activation of synoviolin promoter in rheumatoid synovial cells by a novel transcription complex of interleukin enhancer binding factor 3 and GA binding protein α. Arthritis Rheum 2009;60:63–72.
10. Cooper H, Paterson Y. Preparation of polyclonal antisera. In: Ausubel F, Brent R, Kingston R, Moore D, Seldman J, Smith J, et al, editors. Current protocols in molecular biology. New York: John Wiley & Sons; 1997. p. 11.12.1–11.13.4.
11. Fuller S, Takahashi M, Hurrell J. Preparation of monoclonal antibodies. In: Ausubel F, Brent R, Kingston R, Moore D, Seldman J, Smith J, et al, editors. Current protocols in molecular biology. New York: John Wiley & Sons; 1997. p. 11.4.1–11.11.5.
12. Jiang W, Jimenez G, Wells NJ, Hope TJ, Wahl GM, Hunter T, et al. PRC1: a human mitotic spindle-associated CDK substrate protein required for cytokinesis. Mol Cell 1998;2:877–85.
13. Chung JH, Whiteley M, Felsenfeld G. A 5' element of the chicken β-globin domain serves as an insulator in human erythroid cells and protects against position effect in Drosophila. Cell 1993;74: 505–14.
14. Miyake-Nishijima R, Iwata S, Saijo S, Kobayashi H, Kobayashi S, Souta-Kuribara A, et al. Role of Crk-associated substrate lymphocyte type in the pathophysiology of rheumatoid arthritis in tax transgenic mice and in humans. Arthritis Rheum 2003;48: 1890–900.
15. Brackertz D, Mitchell GF, Mackay IR. Antigen-induced arthritis in mice. I. Induction of arthritis in various strains of mice. Arthritis Rheum 1977;20:841–50.
16. Sellar GC, Jordan SA, Bickmore WA, Fantes JA, van Heyningen V, Whitehead AS. The human serum amyloid A protein (SAA) superfamily gene cluster: mapping to chromosome 11p15.1 by physical and genetic linkage analysis. Genomics 1994;19:221–7.
17. Matsuoka S, Ballif BA, Smogorzewska A, McDonald ER III, Hurov KE, Luo J, et al. ATM and ATR substrate analysis reveals extensive protein networks responsive to DNA damage. Science 2007;316:1160–6.
18. Ballif BA, Villen J, Beausoleil SA, Schwartz D, Gygi SP. Phosphoproteomic analysis of the developing mouse brain. Mol Cell Proteomics 2004;3:1093–101.
19. Coetzee GA, Strachan AF, van der Westhuyzen DR, Hoppe HC, Jeenah MS, de Beer FC. Serum amyloid A-containing human high density lipoprotein 3: density, size, and apolipoprotein composition. J Biol Chem 1986;261:9644–51.
20. Baba S, Takahashi T, Kasama T, Shirasawa H. Identification of two novel amyloid A protein subsets coexisting in an individual patient of AA-amyloidosis. Biochim Biophys Acta 1992;1180: 195–200.
21. Morita Y, Kashihara N, Yamamura M, Okamoto H, Harada S, Kawashima M, et al. Antisense oligonucleotides targeting c-fos mRNA inhibit rheumatoid synovial fibroblast proliferation. Ann Rheum Dis 1998;57:122–4.
22. Samuels J, Krasnokutsky S, Abramson SB. Osteoarthritis: a tale of three tissues. Bull NYU Hosp Jt Dis 2008;66:244–50.
23. Shibakawa A, Aoki H, Masuko-Hongo K, Kato T, Tanaka M, Nishioka K, et al. Presence of pannus-like tissue on osteoarthritic cartilage and its histological character. Osteoarthritis Cartilage 2003;11:133–40.

Takamori et al. Retrovirology 2011, 8:100
http://www.retrovirology.com/content/8/1/100

RETROVIROLOGY

RESEARCH Open Access

Functional impairment of Tax-specific but not cytomegalovirus-specific CD8$^+$ T lymphocytes in a minor population of asymptomatic human T-cell leukemia virus type 1-carriers

Ayako Takamori[1], Atsuhiko Hasegawa[1*], Atae Utsunomiya[2], Yasuhiro Maeda[3,9], Yoshihisa Yamano[4], Masato Masuda[5], Yukiko Shimizu[4], Yotaro Tamai[1], Amane Sasada[1], Na Zeng[1], Ilseung Choi[6], Naokuni Uike[6], Jun Okamura[7], Toshiki Watanabe[8], Takao Masuda[1] and Mari Kannagi[1]

Abstract

Background: Human T-cell leukemia virus type 1 (HTLV-1) causes adult T-cell leukemia (ATL) and HTLV-1-associated myelopathy/tropical spastic paraparesis (HAM/TSP) in a small percentage of infected individuals. ATL is often associated with general immune suppression and an impaired HTLV-1-specific T-cell response, an important host defense system. We previously found that a small fraction of asymptomatic HTLV-1-carriers (AC) already showed impaired T-cell responses against the major target antigen, Tax. However, it is unclear whether the impaired HTLV-1 Tax-specific T-cell response in these individuals is an HTLV-1-specific phenomenon, or merely reflects general immune suppression. In this study, in order to characterize the impaired HTLV-1-specific T-cell response, we investigated the function of Tax-specific CD8$^+$ T-cells in various clinical status of HTLV-1 infection.

Results: By using tetramers consisting of HLA-A*0201, -A*2402, or -A*1101, and corresponding Tax epitope peptides, we detected Tax-specific CD8$^+$ T-cells in the peripheral blood from 87.0% of ACs (n = 20/23) and 100% of HAM/TSP patients (n = 18/18) tested. We also detected Tax-specific CD8$^+$ T-cells in 38.1% of chronic type ATL (cATL) patients (n = 8/21), although its frequencies in peripheral blood CD8$^+$ T cells were significantly lower than those of ACs or HAM/TSP patients. Tax-specific CD8$^+$ T-cells detected in HAM/TSP patients proliferated well in culture and produced IFN-γ when stimulated with Tax peptides. However, such functions were severely impaired in the Tax-specific CD8$^+$ T-cells detected in cATL patients. In ACs, the responses of Tax-specific CD8$^+$ T-cells were retained in most cases. However, we found one AC sample whose Tax-specific CD8$^+$ T-cells hardly produced IFN-γ, and failed to proliferate and express activation (CD69) and degranulation (CD107a) markers in response to Tax peptide. Importantly, the same AC sample contained cytomegalovirus (CMV) pp65-specific CD8$^+$ T-cells that possessed functions upon CMV pp65 peptide stimulation. We further examined additional samples of two smoldering type ATL patients and found that they also showed dysfunctions of Tax-specific but not CMV-specific CD8$^+$ T-cells.

Conclusions: These findings indicated that Tax-specific CD8$^+$ T-cells were scarce and dysfunctional not only in ATL patients but also in a limited AC population, and that the dysfunction was selective for HTLV-1-specifc CD8$^+$ T-cells in early stages.

* Correspondence: hase.impt@tmd.ac.jp
[1]Department of Immunotherapeutics, Tokyo Medical and Dental University, Tokyo, Japan
Full list of author information is available at the end of the article

Background

Human T-cells leukemia virus type 1 (HTLV-1) is the causative agent of a highly aggressive $CD4^+$ T-cell malignancy, adult T-cell leukemia (ATL)[1,2]. As many as 10 million individuals are thought to be infected worldwide, in southern Japan, the Caribbean basin, South America, Melanesia, and equatorial Africa[3]. Unlike human immunodeficiency virus (HIV), the majority of HTLV-1-infected individuals are clinically asymptomatic during their lifetime. However, approximately 5% develop ATL, and another 2-3% develop a variety of chronic inflammatory diseases such as HTLV-1-associated myelopathy/tropical spastic paraparesis (HAM/TSP)[4-8].

HTLV-1-specific cytotoxic T-lymphocytes (CTLs) are thought to play a pivotal role in containing the proliferation of HTLV-1-infected T-cells[9,10]. Tax is known to be the dominant target antigen for HTLV-1-specific CTLs[10-13], and a high frequency of Tax-specific CTLs can be detected in HAM/TSP patients and some asymptomatic HTLV-1 carriers (ACs)[10-14]. However, ATL patients show general immune suppression[15], reduced frequency and dysfunction of Tax-specific CTLs[16,17]. Regulatory T cell (Treg)-like function of $FoxP3^+$ ATL cells and diminished function of dendritic cells may be involved in the immune suppression in ATL patients [18,19], but the precise mechanism is not yet clarified. We previously demonstrated that a fraction of ACs also exhibit reduced T-cell responses against Tax protein [20]. These observations suggest that the reduced HTLV-1-specific T-cell response might be an underlying risk of ATL development, but not the result of ATL. However, it is unknown how the function of HTLV-1-specific $CD8^+$ T-cells becomes impaired in a small percentage of ACs and whether its dysfunction is specific for HTLV-1 antigen or due to general immune suppression.

During chronic stage of infection with several viruses, such as HIV and hepatitis C virus (HCV), virus-specific CTLs gradually lose their cytotoxic activity, the ability to proliferate and secrete a diverse profile of cytokines, ultimately leading to exhaustion, anergy or even deletion of these cells[21-26]. Programmed death-1 (PD-1), a negative regulator in the CD28 superfamily, has recently been shown to be highly expressed on virus-specific T-cells during many chronic viral infections[27-29]. It has also been reported that the interaction of PD-1 with PD-ligand 1 (PD-L1) negatively regulates cytokine production and proliferation of T-cells[30,31]. A previous report indicates that PD-1 is up-regulated on the dominant Tax-specific CTLs in ATL patients and ACs and that immune regulation through the PD-1/PD-L1 pathway may be involved in the dysfunction of HTLV-1-specific CTLs in ATL patients[32].

Studies on memory T-cell differentiation have shown that phenotype, function, and homeostasis of memory T-cells vary for different persistent virus infections[33]. Central memory T-cells (T_{CM}; $CD45RA^-CCR7^+$) are elicited by non-persisting virus that provide transient antigen stimulation, such as in Influenza virus infection. In contrast, effector memory T-cells (T_{EM}; $CD45RA^-CCR7^-$) predominate when relatively high levels of antigen persist, such as in HIV infection. Terminally differentiated memory (T_{Diff}; $CD45RA^+CCR7^-$) can be seen when antigen persists at a low level, such as in cytomegalovirus (CMV) infection. In HTLV-1 infection, it has been reported that dominant Tax-specific CTLs in HAM/TSP patients consist of T_{EM} and T_{Diff} compartments[34].

We previously identified some major epitopes recognized by HTLV-1-specific CTLs in infected individuals carrying HLA-A2, -A11, or -A24[12,35,36]. These allowed us to monitor HTLV-1-specific CTLs and analyze their functions *ex vivo*, by using antigen/HLA tetrameric complexes. In this study, we demonstrate that IFN-γ production and proliferative capacity of tetramer-binding Tax-specific $CD8^+$ T-cells were severely impaired not only in ATL patients but also in a minor population of asymptomatic HTLV-1 carriers (ACs). Importantly, the T-cell dysfunction at the asymptomatic stage was selective for HTLV-1 but not for CMV antigen. In addition, severely impaired HTLV-1-specific but not CMV-specific $CD8^+$ T-cells responses were also observed in patients diagnosed as smoldering ATL, the clinical condition of which is close to that of AC. The dysfunction of HTLV-1-specific $CD8^+$ T-cells in an early clinical stage implies HTLV-1-specific immune suppressive mechanism might be an underlying risk for ATL.

Results

Incidence and frequency of Tax-specific $CD8^+$ T-cells in ACs, and HAM/TSP and cATL patients

In 23 ACs and 18 HAM/TSP and 21 cATL patients carrying HLA-A2, -A11 and/or -A24 alleles, we evaluated the frequencies of Tax-specific $CD8^+$ T-cells by using cognate Tax/HLA tetramers (Figure 1 and Table 1). Tax-specific $CD8^+$ T-cells were detected in 87.0% of ACs and all HAM/TSP patients tested. In contrast, only 38.1% of cATL patients have detectable frequencies of Tax-specific $CD8^+$ T-cells (Table 1). Figure 1B shows that the average frequency of Tax-specific $CD8^+$ T-cells in the $CD8^+$ T-cells of cATL patients (n = 21, 0.90% range: 0%-9.45%) was significantly lower than that in ACs (n = 23, 2.37%, range: 0%-8.23%, $P = 0.0023$). HAM/TSP patients had the highest average frequency of Tax-specific $CD8^+$ T-cells among the three groups (n = 18, 8.88%, range: 1.86%-29.9%, $P = 0.0001$; vs. AC, $P < 0.0001$; vs. cATL patients), which is consistent with

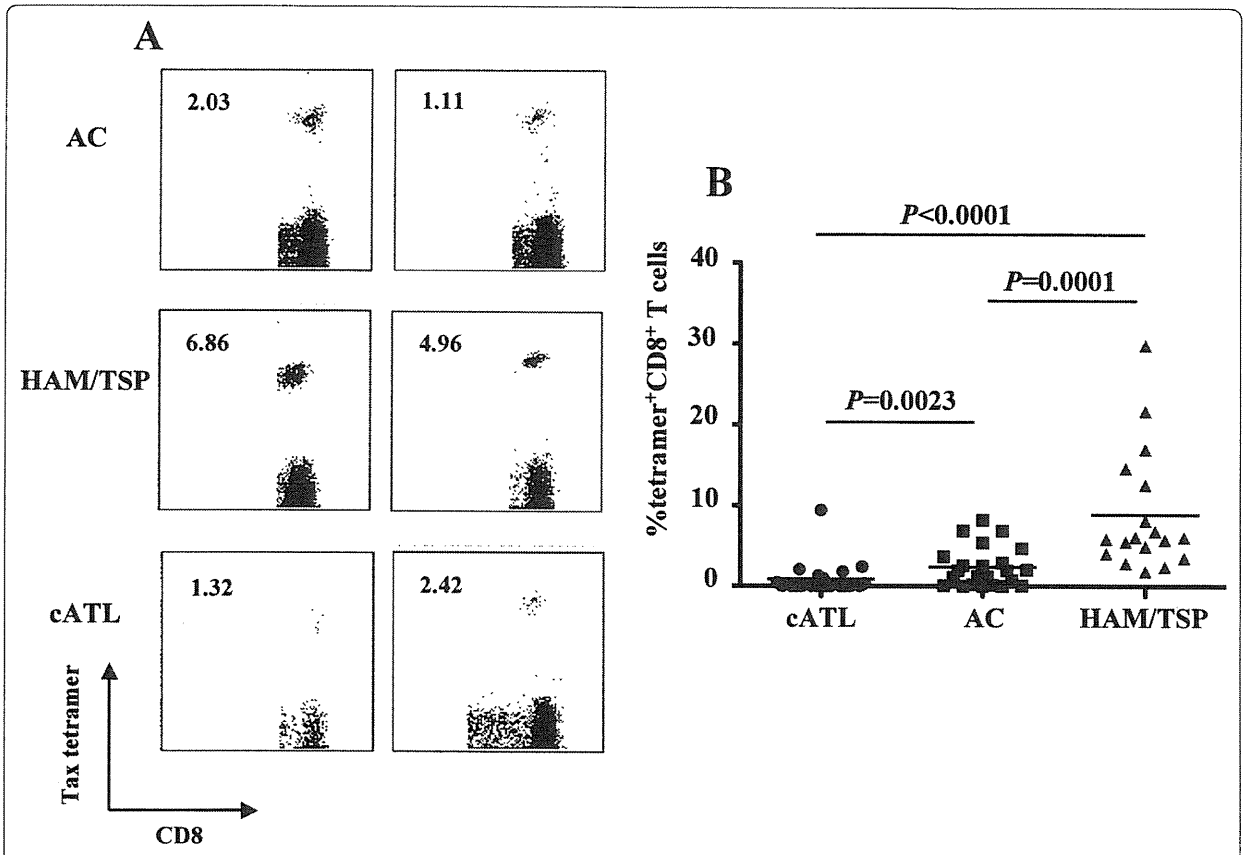

Figure 1 Incidence and frequency of Tax-specific CD8$^+$ T-cells in ACs, and HAM/TSP and cATL patients. (A) Whole blood or PBMCs from AC (top), and HAM/TSP (middle) and cATL (bottom) patients were stained with Tax/HLA tetramer. Number indicates the percentage of tetramer$^+$ cells in CD8$^+$ T-cells. (B) The percentage of Tax-tetramer$^+$ CD8$^+$ T-cells in AC (n = 23), and HAM/TSP (n = 18) and cATL (n = 21) patients. *P* value was determined by the Mann-Whitney *U* test. Horizontal bars indicate the average percentage of Tax-tetramer$^+$ CD8$^+$ T-cells for the group.

previous reports [10,17,37]. It is of note that Tax-specific CD8$^+$ T-cells are detectable even in cATL patients, although the frequency is very low.

Impaired cell proliferation and IFN-γ production of Tax-specific CD8$^+$ T-cells in cATL but not HAM/TSP patients

We next examined IFN-γ production and cell proliferation of Tax-specific CD8$^+$ T-cells in HAM/TSP and cATL patients (Figure 2A). Intracellular IFN-γ staining showed that Tax-specific CD8$^+$ T-cells in all HAM/TSP patients tested produced IFN-γ when stimulated with Tax peptide (Figure 2A). Tax-specific CD8$^+$ T-cells in those HAM/TSP patients proliferated regardless of stimulation with Tax peptide (Figure 2B). In contrast to HAM/TSP patients, IFN-γ production from Tax-specific CD8$^+$ T-cells in a cATL patient was hardly detectable even when stimulated with Tax peptide (4.8%, Figure 2A). In the same donor, Tax-specific CD8$^+$ T-cells

Table 1 The number of blood samples with detectable Tax-specific CD8$^+$ T-cells in all samples tested in this study

Tax/HLA tetramers used in this study	Disease Status		
	AC	HAM/TSP	cATL
HLA-A*0201/Tax11-19	12/14[1]	7/7	2/11
HLA-A*1101/Tax88-96	4/4	4/4	3/5
HLA-A*2402/Tax301-309	13/15	13/13	5/16
No. of tetramer$^+$ samples/total no. of blood samples[2]	20/23 (87.0%)	18/18 (100%)	8/21 (38.1%)

[1] No. of samples with detectable Tax-specific CD8$^+$ T-cells/total no. of samples carrying each HLA allele. When the frequency of tetramer$^+$ cells was more than 0.04% of CD8$^+$ T-cells, the sample was regarded as detectable.

[2] In case Tax-specific CD8$^+$ T-cells was detectable by either tetramer in a sample carrying two of three HLA-A alleles above, the sample was regarded as positive.

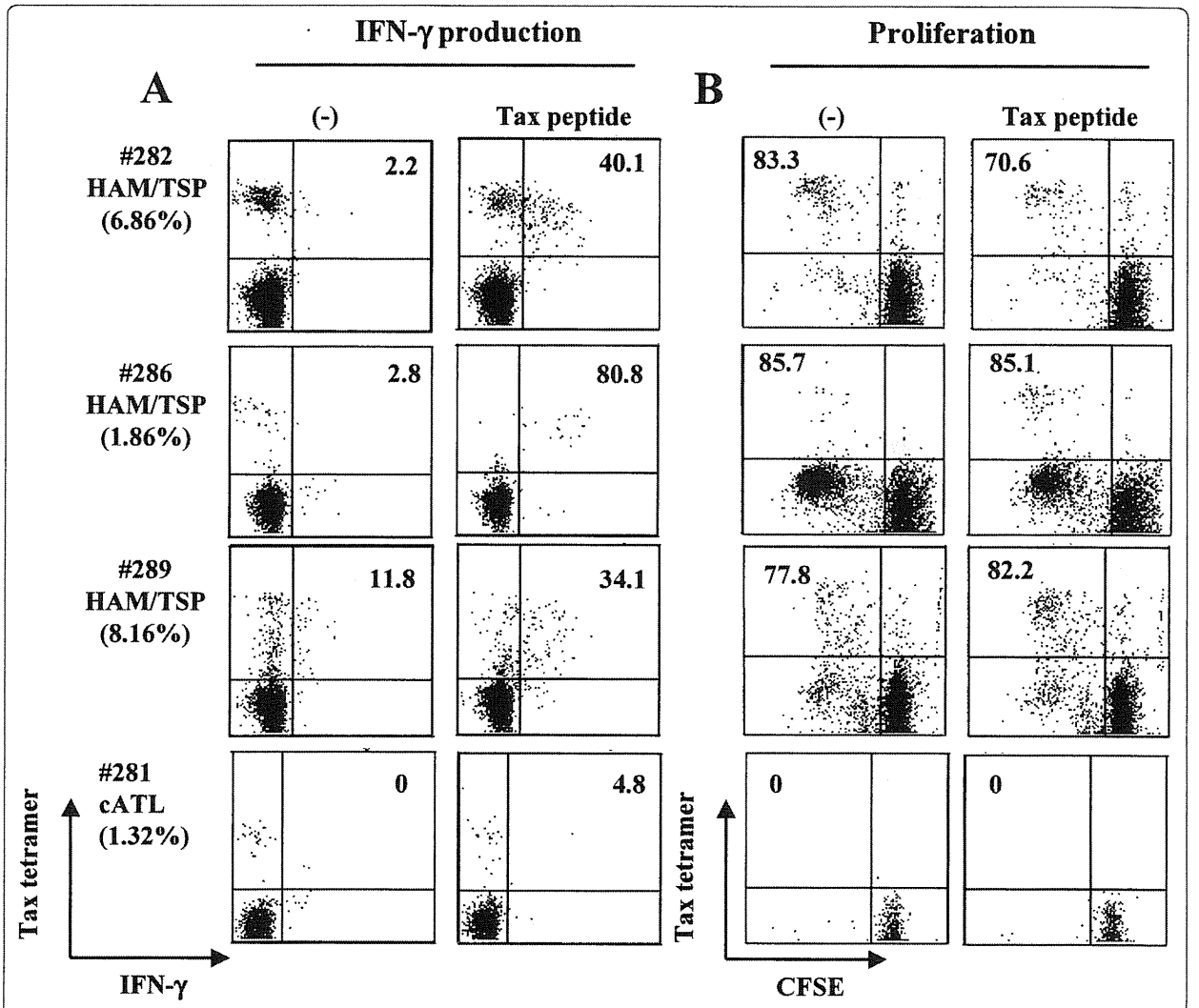

Figure 2 IFN-γ production and proliferation of Tax-specific CD8$^+$ T-cells in HAM/TSP and cATL patients. (A) PBMCs from HAM/TSP and cATL patients were stimulated with or without 10 μM Tax peptide for 6 hrs. The number indicates the percentage of IFN-γ-producing cells in tetramer$^+$ cells. (B) For CFSE-based T-cell proliferation, CFSE-labeled PBMCs from HAM/TSP and cATL patients were cultured in the presence or absence of 100 nM Tax peptide for 6 days. The number indicates the percentage of dividing (CFSE^{low}) cells in tetramer$^+$ cells. The percentage of tetramer$^+$ cells among CD8$^+$ T cells in fresh blood is indicated in parenthesis under the patient ID.

could be detected in fresh blood (1.32%) and after 6 hrs incubation as shown in Figure 2A, but not after 6 day-culture, suggesting that Tax-specific CD8$^+$ T-cells in this cATL patient had no proliferative capacity (Figure 2B). We tested PBMC from four other cATL patients who had detectable Tax-specific CD8$^+$ T-cells, but none of them showed proliferation of Tax-specific CD8$^+$ T-cells by either the CFSE-based proliferation assay or 13-day culture (Additional file 1). Collectively, these results indicate that Tax-specific CD8$^+$ T-cells from most cATL patients are impaired in their capacities to proliferate and produce IFN-γ.

Diversity in the IFN-γ production and cell proliferation of Tax-specific CD8$^+$ T-cells in ACs

Our recent studies using the GST-Tax protein-based assay demonstrated that the extent of Tax-specific T-cell responses varied widely in ACs[20]. We then evaluated proliferation and/or IFN-γ production of tetramer-binding Tax-specific CD8$^+$ T-cells in 14 ACs (Table 2). Representative data on 4 of 14 ACs are shown in Figures 3A and 3B. In 3 ACs (#251, #313, and #360), Tax-specific CD8$^+$ T-cells produced IFN-γ and proliferated in response to Tax peptide (Figures 3A and 3B). Similarly to HAM/TSP samples, a large proportion of Tax-